Nationaal Lucht- en Ruimtevaartlaboratorium

National Aerospace Laboratory NLR

.

Optimisation and evaluation of an Active Gurney Flap system for rotorcraft performance improvement and its impact on handling qualities

S.C. van 't Hoff, M.P.C. van Rooij, F. Federico, A. Visingardi and M.D. Pavel

Executive summary

Optimisation and evaluation of an Active Gurney Flap system for rotorcraft performance improvement and its impact on handling qualities

Problem area

The Green Rotorcraft Integrated Technology Demonstrator strives to develop technologies that will reduce the fuel consumption and noise footprint of the future European helicopter fleet. One of the technologies that is under development in the Innovative Rotor Blades work package is the Active Gurney Flap (AGF) concept. This concept is based on the active deployment of a small Gurney Flap at the bottom side of the trailing-edge of the main rotor blade airfoil. The additional lift provided by the system can be applied towards a multitude of objectives, but in this context the system is used to achieve reductions in power consumption, while simultaneously attempting to minimize the negative impact on cockpit vibrations and handling qualities.

Description of work

In the initial stages of this research initiative, the focus has been on developing a low-cost empirical model to capture the two dimensional unsteady aerodynamic effects of the AGF system. This model has subsequently been used in an optimization study, to determine the optimum radial position of the finite-span AGF element, as well as an open-loop control schedule that allows maximum power reductions without negatively impacting the cockpit vibrations. Finally, a parameter investigation was made to investigate the effect of the AGF system on handling qualities, based on the ADS-33 attitude quickness parameter.

Results and conclusions

It has been shown that, at least conceptually, the AGF system is capable of achieving significant power reductions in level forward flight. The potential for power reduction increases with the disc loading and decreases with airspeed. The impact on handling qualities is generally limited, but care must be taken in the selection of the control schedule, as an improper combination of control parameters may lead to degradation in attitude quickness.

Applicability

Advanced active rotor systems such as the AGF concept are the spearhead of current helicopter R&D efforts. It is vital for NLR to stay abreast of such developments.

This report is based on a presentation held at the European Rotorcraft Forum, Moscow, September 3-6, 2013.

Optimisation and evaluation of an Active Gurney Flap system for rotorcraft performance improvement and its impact on handling qualities

NLR-TP-2013-577

Optimisation and evaluation of an Active Gurney Flap system for rotorcraft performance improvement and its impact on handling qualities

S.C. van 't Hoff, M.P.C. van Rooij, F. Federico[1], A. Visingardi[1] and M.D. Pavel[2]

[1] CIRA

[2] TU Delft

Summary

In the framework of the Clean Sky - Green Rotorcraft ITD, CIRA, NLR and TU Delft are involved in a common research initiative to study the potential of Active Gurney Flap (AGF) systems to reduce the required power of a medium size helicopter with a minimum impact on vibrations and handling qualities. CIRA and NLR have implemented two different empirical AGF models into the commercial comprehensive rotorcraft analysis code FLIGHTLAB, allowing detailed aeroelastic and performance analyses. On their part, TU Delft integrated a simplified AGF model into an in-house nonlinear flight mechanics code geared towards handling qualities assessment. In the first part of this paper a comparison is made between CFD and the empirical models employed by the different organizations to capture the 2-D unsteady aerodynamic effects of the AGF system. Despite the relative simplicity of the empirical models, a reasonable correlation is achieved, even when considering a time varying freestream. The second part of the paper presents an optimisation study aimed at finding the optimum radial position of the AGF system, as well as defining an open-loop control schedule intended to maximise the power reductions without exacerbating the vibrations in level forward flight. Finally, the paper concludes with a parametric evaluation of the impact of a generic AGF system on rotorcraft handling qualities. It is found that the AGF system moves the quickness in pitch towards Level 1 handling qualities at low airspeeds and towards Level 2 handling qualities at high airspeeds.

Contents

Nomenclature

α	Angle of attack
c	Airfoil chord
C_d	Drag coefficient
C_l	Lift coefficient
C_m	Pitching moment coefficient
C_w	Thrust coefficient
$\Delta\theta_{pk}$	Peak manoeuvre pitch attitude change
$\Delta\psi$	AGF deployed period
h	Gurney flap height
k	Reduced frequency, $k = \omega c/2V$
λ_i	Inflow ratio
M	Mach number
n_{zpk}^{vib}	Peak amplitude of vertical hub shear
μ	Advance ratio
p	Body roll rate
q	Body pitch rate
q_{pk}	Peak manoeuvre pitch rate
Q_l	Load quickness parameter
Q_θ	Theta quickness parameter
r_{AGF}	AGF radial station
R	Main rotor radius
Re	Reynolds number
σ	Density ratio
σ_r	Main rotor solidity
t	Dimensional time
t_δ	Deployment/retraction time
θ	Body pitch attitude
V	Forward flight speed
v_i	Induced velocity
$\ddot{x}^{4P}$	4/rev pilot seat vibration acceleration
ψ_{out}	AGF deployment azimuth
ψ_{in}	AGF retraction azimuth
Ω	Main rotor speed

This page is intentionally left blank.

1 INTRODUCTION

In recent years there has been a lot of research on active rotor system concepts aimed at the reduction of rotor power consumption and vibrations, or the alleviation of dynamic stall. Among the contending technologies is the Active Gurney Flap (AGF) concept, where a small flap (also referred to as a Miniature Trailing-Edge Effector) is deployed near the trailing-edge on the pressure side of the airfoil, orthogonal to the surface (see Figure *1*). The main advantages of the AGF concept over the myriad of competing technologies are its relatively low actuation force and power requirements. The challenge in realizing such a system lies mostly in the design of an actuation mechanism that can cope with the high centrifugal loads and elastic blade deformations, while allowing for a maximum deployment height.

Recent studies have investigated the potential of AGF systems towards helicopter power[2-4], noise and vibration reduction[5,6]. In some cases these metrics are considered in an isolated manner, with at times little attention to the practical limitations on the implementation of the system. As recognised by Liu *et al.*[7], the viability of an active rotor concept on a production helicopter in a practical setting requires the combined evaluation of the aforementioned aspects. The present study attempts to present a comprehensive investigation by jointly considering the effects of the AGF system on rotor power consumption, vibrations and handling qualities. Noise reduction is not explicitly considered, but could also be achieved by taking advantage of the performance margin afforded by the AGF system to reduce the main rotor speed.

The present investigation considers a ramped open-loop control concept aimed at power reduction. Deployment is assumed to occur only on the retreating side of the rotor disk to avoid the increased drag penalty of Gurney flaps at high Mach numbers. The optimum radial position of the AGF system is derived using a multi-point single-objective optimisation. Next, the active control schedule is optimised to achieve maximum performance benefit without negatively affecting the vibration levels using multiple single-point multi-objective optimisations distributed over the (level) flight envelope. Finally, the AGF system is evaluated in terms of its impact on the handling qualities of a medium size helicopter.

This study has been performed in the context of the European Clean Sky Joint Technology Initiative, where the Innovative Rotor Blades work package is striving to develop a full-scale AGF system that is aimed at the reduction of rotorcraft noise and power consumption. The design features a single-element AGF system with an electromechanical actuator. The system will be tested for the first time in a 2-D environment at the end of 2013 and is scheduled to be flight tested at a future date.

2   MODELLING

2.1   2-D aerodynamics

2.1.1   NLR

The 2-D model of the unsteady AGF aerodynamics employed by NLR is based on the work of Vieira et al.[8]. To facilitate the implementation into FLIGHTLAB, the model has been transformed to a state-space format. The AGF model itself is an adaptation of the unsteady conventional trailing-edge flap model developed by Hariharan-Leishman[9], which is based on indicial response methods. Under compressible conditions, the plain flap model uses an exponential approximation to the Wagner function to predict the transient between the initial (non-circulatory) and asymptotic (circulatory) aerodynamic response. In case of a plain flap, analytical expressions exist for both extremes of the response. Conversely, for Gurney flaps, the circulatory steady-state response can be derived from CFD or wind tunnel test results. The non-circulatory effects are neglected. Similar to the plain flap case, the circulatory (shed wake) transient response can be captured by an exponential approximation, the coefficients of which can be derived from CFD or wind tunnel data.

The aerodynamic response of an AGF positioned upstream of the trailing-edge is characterised by a vortex shedding event that can introduce an adverse peak in the initial lift and pitching moment response. The magnitude and time scale of this peak depends on the reduced frequency of the deployment

and the chordwise offset of the flap from the trailing-edge. The associated vortex lift is modelled as suggested by Vieira et al.[8], while the pitching moment is modified as proposed by Roedts et al.[3].

As recognised by Kinzel[2], the unsteady aerodynamic response of deploying and retracting Gurney flaps differ significantly. As a result, the parameters of the empirical AGF model have to be scheduled according to the actuation state, taking care to avoid discontinuities in the response. Additionally, the vortex lift and pitching moment effects have to be removed during the retraction phase.

The AGF model has been integrated into the Leishman-Beddoes dynamic stall model available in FLIGHTLAB[10]. To account for the effect of the Gurney flap on the dynamic stall behaviour of the airfoil, the dynamic stall model interpolates between two parameter sets; one for the clean airfoil and one for the flapped airfoil. The modifications are limited to the (five) dynamic parameters of the Leishman-Beddoes dynamic stall model in order to retain the airfoil static stall curves. The effect is generally limited to a minor reduction of the dynamic stall angle and a delayed reattachment.

Since the model is intended to be used also in stall conditions, the quasi-steady increments due to Gurney flap deployment must be a function of angle of attack. The delay in the circulatory response is accounted for by performing the table lookup of the static

Gurney flap airloads using the effective (delayed) angle of attack of the attached flow solution provided by the Leishman-Beddoes model.

2.1.2 CIRA

The 2-D unsteady AGF aerodynamics model used by CIRA is based on the approach proposed by He et al.[11,12] and is available in the latest release of FLIGHTLAB. Following this method, the basic unsteady airloads formulation is refined with explicit expressions to account for the presence of a generic time-varying airfoil camber.

The proposed approach is ideally suited to work in conjunction with the fundamental formulation of the Leishman-Beddoes dynamic model and covers any type of airfoil control such as: dynamic trailing edge flap, leading edge droop and Gurney flap.

The dynamic camber approach has been implemented in FLIGHTLAB to model the AGF system. Similar to the approach adopted by NLR, the model linearly interpolates between two sets of Mach number dependent parameters: one for the clean airfoil and one for the flapped airfoil. In this case, however, the interpolation between the clean and the flapped airfoil parameters is a function of the effective angle of attack which reflects the airfoil camber change associated with the AGF actuation.

2.1.3 Comparison with CFD

Steady-state aerodynamics

The steady-state aerodynamic response for different deployment heights is introduced in the NLR model through table-lookup of time-averaged 2-D URANS CFD results as a function of angle of attack and Mach number. Figure 2 to Figure 4 show the lift, drag and pitching moment for a NACA-23012 airfoil equipped with a Gurney flap located at 95% chord at $M = 0.4$. In the linear region, the lift and drag responses follow roughly the relations for incompressible flow suggested by Bae et al.[4]:

$$(1) \qquad \Delta C_l \propto \left(\frac{h}{c} \right)^{\frac{1}{2}}$$

$$(2) \qquad \Delta C_d \propto \left(\frac{h}{c} \right)^{\frac{3}{2}}$$

The constant of proportionality is found from available data at a specified value of h/c and can show significant airfoil dependency.

As indicated by the relations above and also by Figure 5, the lift to drag ratio decreases for increasing deployment height. Additionally, the presence of the Gurney flap reduces the positive static stall angle. The Gurney flap becomes ineffective beyond negative stall. The aft loading generated by the Gurney flap results in a significant increase in the magnitude of the static pitching moment.

Finally, as shown by Kinzel[2], the lift to drag ratio is increasingly deteriorated as the Mach number increases beyond $M = 0.4$ and compressibility effects become more prominent. For the purpose of this study, CFD data was generated up to $M = 0.5$, which is sufficient when it is assumed the AGF system

Dynamic stall

To evaluate the behaviour of airfoils equipped with an AGF in dynamic stall conditions, CIRA performed several 2D URANS CFD computations of pitching airfoils using their in-house Navier-Stokes solver ZEN[13,14]. Fully turbulent calculations were performed using Menter's κ–ω SST turbulence model on structured computational meshes of 145088 cells. Each dynamic stall cycle consists of 2048 time steps. The effect of turbulence modelling and laminar-turbulent transition on the dynamic stall behaviour[15] was not considered in great detail.

In order to simulate the presence of an AGF and the time variation of its length, the Gurney flap was modelled as a solid wall of zero thickness and time varying length. A wall normal grid line was used to apply the no-penetration boundary condition.

To replicate the dynamic stall behaviour of both the clean and flapped airfoils, CIRA has adopted the Leishman-Beddoes dynamic stall model. A MATLAB-based optimisation procedure was set-up in order to tune the parameters of the Leishman-Beddoes model. The objective function of the optimisation is based on a comparison with CFD data at a specified number of characteristic points. A residual function has been defined in order to drive the optimisation toward the final goal. The points used to define the residuals are: the maximum lift coefficient during the upstroke phase; the relative maximum during the

down-stroke phase (corresponding to the onset of reattachment); the minimum lift coefficient; the skin-friction drag; and the zero-lift pitching moment coefficient. The residual takes the following form:

$$r = \sum_{i=1}^{N} \Delta_i$$

(3)

$$\text{where } \Delta_i = \sqrt{\left(\Delta C_i\right)^2 + \left(\Delta \alpha_i\right)^2}$$

which expresses the sum of the distances between the CFD and Leishman-Beddoes data over the N characteristic points in terms of the generic aerodynamic coefficient C and the angle of attack α.

To verify the (clean airfoil) CFD calculations and the implementation of the Leishman-Beddoes model, the procedure described above was applied to the dynamic stall of a NACA-0012 airfoil at $M = 0.4$ and $Re = 8$ million ($\alpha = 10° + 8° \sin (2kt)$, $k = 0.075$) for which experimental results are available. The comparison is illustrated in Figure 6 to Figure 8 for the three aerodynamic coefficients. The CFD computations do not quite capture the reattachment process and there are some discrepancies in the peak drag and pitching moment values. The Leishman-Beddoes model provides a reasonable approximation given its relatively simple formulation.

To verify the performance of the empirical AGF models in a dynamic stall condition, the same procedure has also been applied to an ARO-212 airfoil with a Gurney flap that is actively deployed during the dynamic stall cycle.

Figure 9 illustrates the results of the numerical simulation of the lift coefficient in dynamic stall conditions at a Mach number of $M = 0.4$. The AGF is located at 95% of the chord and has a maximum deployment height of 3% of the chord length. In the absence of static stall CFD results for the ARO-212 airfoil, the CIRA model, tuned to the dynamic results, was used to generate the static parameters required by the NLR model.

The empirical models show a reasonable correlation with the CFD data, at least in terms of maximum lift and stall angle. As is typical for dynamic stall calculations, the reattachment process is more difficult to match.

Time-varying freestream Mach number

To investigate the effect of a time-varying free stream Mach number, NLR performed 2D URANS CFD computations using ENSOLV[16], an in-house code for aerodynamic, aeroelastic and aeroacoustic calculations used at NLR. Turbulence was incorporated by means of the TNT variant of the two-equation k-ω turbulence model, extended with an Explicit Algebraic Reynolds Stress Model[17,18] The number of time steps per rotor revolution was set to 3600, equivalent to 0.1° azimuthal rotation per time step. The Gurney flap was modelled by applying a wall boundary condition along a grid line. A morphing grid line method was also implemented to simulate more complex flap protrusion schedules. The results presented here, however, correspond to a simple cosine ramp orthogonal deployment.

To minimise the complexity of the prevailing flow phenomena, the variation of angle of attack and Mach number was selected such that dynamic stall is avoided. The Mach number variation was achieved in the CFD computations by superimposing a fore-aft (lead-lag) motion of the airfoil on a constant Mach number freestream. This simplification is typically considered suitable for the range of reduced frequencies encountered on helicopter main rotor blades[19].

Figure 10 to
Figure 12 present the lift, drag and pitching moment on an oscillating NACA-23012 airfoil with a deploying Gurney flap in a freestream with time-varying Mach number. To remove the dependency on the prediction of the clean airfoil response, the increments due to the AGF have been added to the clean airfoil CFD results. The angle of attack and Mach number variations follow roughly:

$$\alpha = 6.5° - 5.5° \sin(\Omega t)$$
$$M = 0.4 + 0.2 \sin(\Omega t)$$

The main rotor speed equals $\Omega = 26.26$ rad/s. With a chord equal to $c = 0.65$ m, this gives an average reduced frequency of $k = 0.063$.

The models show a good overall correlation with the CFD results. The model employed by CIRA shows a small peak in the initial lift response related to apparent non-circulatory effects that are ignored in the NLR model. The initial drag peak, which has a magnitude of almost four times the steady drag and which dominates the drag response for

practically the entire deployment phase, is captured by both models. The drag peak towards the end of the deployed phase is underestimated by both models. The NLR model also shows a slightly delayed lift decay in the same period. The result is a somewhat optimistic prediction of the performance of the AGF system during part of the rotor revolution. Nevertheless, the correlation achieved is reasonable and the predictive capability compares favourably with that of the dynamic stall formulation in which the models are integrated.

2.2 Flight mechanics

2.2.1 NLR

The NLR study is based on a UH60-like medium size helicopter. The main rotor blades feature a constant NACA-23012 airfoil along the blade length with an AGF section that can be arbitrarily positioned along the length of the blade. In order to accurately capture the effect of the AGF on the vibration levels and power consumption, the model includes a finite element representation of the main rotor blades with coupled flap, lag and torsion dynamics and a time-accurate periodic prescribed vortex wake inflow model. The inclusion of blade torsion dynamics is essential for capturing the non-negligible elastic twist response to AGF deployment.

When using 2-D unsteady airfoil models in conjunction with a dynamic inflow or vortex wake model, care must be taken not to omit or duplicate the shed wake effects[20]. Since the shed wake effects are an inherent part of the

AGF model it has been opted to exclude the AGF loads from the rotor induced velocity calculations. Conversely, the shed wake effects of the Leishman-Beddoes dynamic stall model have been removed and are instead accounted for by the wake model.

The stiffness properties of the main rotor blades do not explicitly account for the presence of the AGF system. The additional weight is included by the introduction of a distributed mass of 5 kg with zero chordwise offset from the quarter chord. No attempt has been made to tailor e.g. the blade torsion frequency to maximise the efficiency of the AGF system.

Three-dimensional steady incompressible CFD results by Lee *et al.*[21] indicate that edge-effects for finite width Gurney flaps are minimal for span-height ratios above 2.0. The flap effectiveness is therefore assumed to be 100%. The Gurney flap is assumed to be rectangular. No attempt has been made to obtain drag reductions through 3-D shaping. Gurney flap segmentation, such as might be required to cope with large blade deformations, is also not considered.

2.2.2 TU Delft

The handling qualities study performed by the Delft Technical University is based on an in-house 13 degrees of freedom generic flight mechanics model for conventional helicopters[22]. The rotor blades are assumed to be rigid and are modelled through an equivalent hinge offset matching the first flap and lag frequencies. The model includes a 6-

dof rigid body, 3-dof first order flapping (disk tilt) dynamics, 3-dof Pitt-Peters main rotor dynamic inflow and 1-dof quasi-steady dynamic inflow for the tail rotor. The rotor disk tilt dynamics has been expressed using Lagrange equations, allowing for high-order non-linear coupling effects between the flapping and body degrees of freedom which may affect the flight mechanics predictions. Usually, such higher-order terms are neglected in flight mechanics approximations. However, the terms may affect the flight mechanics behaviour, especially during manoeuvring flight where coupled non-linear effects increase. The ordering scheme as used in the model is given in Table 1. The table presents the order of the advance ratio components (μ_x, μ_y, μ_z), the dynamic inflow coefficients $(\lambda_0, \lambda_s, \lambda_c)$ and the pitch and roll rates (p, q) in the model.

Piloted simulation modelling typically concentrates on intermediate and slow time-scales, as this corresponds to the steady-state flapping motion of the rotor. The fast blade motions are usually neglected and the blade is assumed to respond instantaneously to control inputs, pitch motion and helicopter velocity. In this model, first order flapping (disk tilt) dynamics has been added to the body dynamics. The rotor disk tilt dynamics is derived using concepts originating from classical lifting line theory. In the case of a helicopter rotor blade, the straightforward application of this theory is questionable since the blade sections encounter unsteady and yawed flow. Therefore, in the modelling of the AGF rotor this assumption has been removed and the formulae for the disk tilt angles have been corrected to account for the effects of unsteady and swept flow. The correction is based on the formulation presented by Van Holten[22,23], using a sweep correction factor in the rotor disk tilt angles that accounts for the sweep effect in relation to lift.

Table 1: A sample of the ordering scheme used in the TU Delft flight mechanics model

x	x_{min}	x_{max}	$unit$	$\bar{x}$	$\overline{\lvert x \rvert}$
u	-30	80	m/s	$\mu_x = \dfrac{u}{\Omega R}$	.5
v	20	20	m/s	$\mu_y = \dfrac{v}{\Omega R}$	.1
w	-30	16	m/s	$\mu_z = \dfrac{w}{\Omega R}$	.15
v_{i0}	2	15	m/s	$\lambda_0 = \dfrac{v_{i0}}{\Omega R}$	.075
v_{is}	-5	5	m/s	$\lambda_s = \dfrac{v_{is}}{\Omega R}$	.115
v_{ic}	-10	10	m/s	$\lambda_c = \dfrac{v_{ic}}{\Omega R}$	.23
p	-1	1	rad/s	$\bar{p} = \dfrac{p}{\Omega}$	.05
q	-1	1	rad/s	$\bar{q} = \dfrac{q}{\Omega}$	.05

2.3 Optimisation

The optimisation architecture employed by NLR to optimise the AGF system is based on a Kriging surrogate aided search of the objective space, the basic theory of which in the work of Forrester[24]. Starting from an initial static random space filling (best Latin hypercube) sampling of the variable space, an evolutionary optimisation algorithm is used to find the next dynamic sample with the highest Expected Improvement. In case of a multi-objective formulation, an Expected Maximin Improvement method proposed by Svenson[25]

is used instead. All objectives are normalised between zero and unity, where zero equals the current optimum.

Each time the radial position of the AGF system is updated, the radial aerodynamic discretisation changes. To remove the sensitivity of the optimum to the aerodynamic discretisation, the configuration is evaluated each iteration for both the baseline and active rotor case. The objective function is then found as the ratio of the two results.

At each iteration, the FLIGHTLAB model is called by the optimisation routine to trim the aircraft in a level forward flight. In order to avoid tight trim tolerances, the Kriging surrogates are extended with a regression constant that reduces the sensitivity of the optimisation process to small variations in the evaluation of the objective function.

The objective of the optimisation is to minimise the power consumption without negatively affecting the 4/rev vibrations. Higher harmonic deployment is typically adopted in vibration reduction studies and has also been shown to be beneficial for performance enhancement[7]. In this case, however, the optimisation assumes a deployment cycle where the AGF is deployed and retracted following smooth cosine ramps on the retreating side of the rotor disk. Note that the higher harmonic content of this type of ramped deployment is non-negligible and will affect the 4/rev vibrations in the fixed frame. A summary of the optimisation

constraints adopted for this study are presented in Table 2.

Table 2: Optimisation constraints

Variable	Bounds
Radial location, r_{AGF} [r/R]	0.2-0.4 / 0.8-1.0
Deployment height, h/c [%]	0 / 1.2
Deployment time, t_δ [ms]	10 / 20
Deployment azimuth, $\psi_{out/in}$ [deg]	180 / 360

3 RESULTS

3.1 Performance

3.1.1 Multi-point optimisation

To determine the optimum radial location of the AGF system, a multi-point optimisation has been performed where the required power in two flight conditions form the optimisation objectives. The flight conditions adopted for the optimisation are summarised in Table 3 and have been selected with the aim of achieving a globally efficient solution. The power reductions achieved are also indicated in the table.

Table 3: Flight conditions adopted for multi-point optimisation

Objective	μ	Cw/σr	ΔP [%]
J_1	0.19	0.12	-8.8
J_2	0.39	0.08	-3.4

Given the constraints defined for the optimisation it turns out that the optimum

solutions for both flight conditions lie very close together. A good trade-off for the optimum radial position of the AGF is found to be 0.7-0.9 *r/R*, with maximum deployment over the entire retreating side of the rotor disk. Moving the AGF further outboard deteriorates the performance in the high speed flight condition.

The power difference between the baseline and active rotor is presented in Figure 13 and Figure 14 for both flight conditions. Negative levels (i.e. power reductions) are indicated by dashed contour lines. In both cases there is an off-loading of the tip on the retreating side of the disk, as well as in parts of the 3rd and 4th quadrants. A large part of the remainder of the disk also shows small power savings which can be attributed to a reduction in the effective angle of attack in all but the 2nd quadrant, as can be seen in Figure 15 and Figure 16.

3.1.2 Multi-objective optimisation

To evaluate the performance of the AGF system in terms of both power consumption and vibrations, the previously determined optimum configuration has been tested across the flight envelope without any open-loop scheduling of the AGF control variables (i.e. deployment height, speed and phase), considering only level forward flight at moderate to high speeds.

As can be seen in Figure 17 the power reductions reported in the previous section are representative for the performance across the remainder of the envelope. The potential for power reductions is lowest at high speeds and

low thrust values where the AGF lift to drag ratio is relatively low and the main rotor is relatively far removed from its stall boundary.

The effect of the unscheduled AGF system on the vector norm of the 4/rev pilot seat vibrations in level forward flight is presented in Figure 18. The vibrations are reduced at the high speed end of the envelope where the unsteady aerodynamic environment results in relatively high vibration levels. At moderate advance ratios, however, there are regions of significant increase in the 4/rev vibrations.

To tune the performance of the AGF system, several local optimisations were performed in order to define an open-loop control schedule that maximises the achievable power reduction while restricting the vibrations to levels equal to or below the baseline. A sample of the Pareto fronts for two advance ratios at different blade loadings is presented in Figure 19. In practically all cases the Pareto front features a plateau where power reductions can be obtained with minimal impact on the 4/rev vibrations. In the cases where this plateau lies above the baseline rotor vibration level (i.e. objective 2 is larger than unity) the constraint on vibrations results in an unfavourable trade-off. Nevertheless, even in such cases reasonable power reductions remain.

The scheduled open-loop performance in terms of the remaining power reductions and 4/rev vibrations can be found in Figure 20 and Figure 21. The near baseline vibration levels

17

are achieved at the expense of a moderate reduction in performance in the range of 0-2% in most flight conditions. Hence, even with constraints on the allowable vibrations, the AGF system has a significant potential for power reductions over a large part of the level flight envelope. The associated open-loop control schedule is presented in Figure 22 and Figure 23. The figures show that, in order to attenuate the 4/rev vibrations, the AGF deployment is shifted towards the 4th quadrant. The delay in deployment increases with airspeed up to an advance ratio of $\mu =$ 0.31. In the conditions where the unscheduled active rotor shows an especially large increase in vibrations, the deployment is further restricted by shifting the retraction to lower values of azimuth, resulting in a deployment which is roughly symmetrically distributed over the 3rd and 4th quadrants.

3.2   Handling qualities

In order to investigate the effects of an AGF rotor on helicopter handling qualities, it was decided to conduct a controllability study using temporal analysis as presented in the Aeronautical Design Standard ADS-33[27]. To maintain generality, the investigation considers several parametric variations of a generic AGF configuration.

The analysis is focused on the quickness parameter, which is a measure of the angular speed peaks obtained with moderate amplitude attitude changes. Quickness (in roll, pitch or yaw) is an innovative measure defined by the ADS-33 to measure the helicopter's ability to achieve rapid and

precise attitude changes when performing a sharp pitch/roll/yaw manoeuvre. From a handling qualities point of view, high quickness is associated with strong manoeuvre capability[28]. From a pilot point of view, when the quickness parameter is too low it means that the aircraft is too sluggish for tracking-type tasks; quickness that is too high results in pilots complaining of jerkiness or over-sensitivity. In fact, quickening the manoeuvre will mean that the pilot achieves the demanded peak quicker and will require the use of less control and anticipation. Less quickness requires more anticipation from the pilot and thus a more complex control strategy. This will lead to an increase in workload and degradation in the pilot judgement of handling qualities.

For example, the pitch attitude quickness parameter (theta quickness) Q_θ is defined as the ratio of the maximum pitch rate q_{pk} to the peak pitch attitude angle change $\Delta\theta_{pk}$ achieved during that manoeuvre (see Figure 24), that is:

(4) $Q_\theta \stackrel{\text{def}}{=} \frac{q_{pk}}{\Delta\theta_{pk}}$ [1/sec]

ADS-33 defines handling qualities boundaries for the attitude quickness parameter as a function of the minimum attitude change $\Delta\theta_{min}$, see Figure 24.

Pavel and Padfield[29] proposed a complementary metric, the so-called vibratory quickness parameter, to characterise the vibratory loads in the rotor as:

(5) $Q_l \stackrel{\text{def}}{=} \frac{n_{zpk}^{vib}}{\Delta\theta}$ [1/deg]

where $n_{zpk}{}^{vib}$ represents the peak amplitude of the vibratory components of the hub shears in g units, see Figure 25. While the attitude quickness characterises the helicopter performance during manoeuvring flight, the load quickness parameter is used to quantify the build-up of loads in the rotor and can be used for parallel performance enhancement and structural load alleviation. The present paper applies the same vibratory load quickness to the AGF rotor.

To illustrate the process of mapping the quickness parameter for an AGF rotor, consider first the kinematics of a manoeuvre in the pitch axis to a change in aircraft attitude. Figure 26 presents the pitch angle and pitch rate transients in response to a 2 second pulse input on the longitudinal stick for a helicopter with and without an AGF system (assuming for the moment $r_{AGF} = 0.6$-$0.8R$, $\psi_{out} = 210$-$220°$, $\psi_{in} = 330$-$340°$). The delta symbols in the figure indicate the peak and minimum pitch attitude change and rate. The minimum pitch change $\Delta\theta_{min}$ in a pulse manoeuvre in forward flight is defined as the value of the pitch attitude corresponding to the time at which 10% decay from the maximum pitch rate q_{pk} is achieved. Using this definition, a series of pulse inputs were flown with the TU Delft model, varying the pulse duration and the initial forward airspeed. Figure 27 illustrates the pitch attitude quickness charts for the pulses flown in the helicopter with a passive rotor. The ADS-33 Level 1/2 boundary for a general mission task element is also plotted in the figure for reference. The characteristic

exponential shape of the quickness parameter with increasing pulse duration can be recognised in the figure. It can be observed that as the pulse duration is increased, the quickness decreases into the Level 2 handling qualities (HQs) region. Also, as the airspeed increases, the quickness charts move further towards level 2 HQs.

To study the effect of a generic AGF system on the theta quickness of the aircraft, a parameter study has been performed considering different control configurations. Firstly, assume a fixed deployment azimuth corresponding to $\psi_{out} = 210$-$220°$, $\psi_{in} = 330$-$340°$. Figure 28 through Figure 32 present the quickness charts for the same pulses as previously applied for the passive rotor case, with the AGF spanwise position varying as: 0.3-0.5R, 0.4-0.6R, 0.5-0.7R, 0.6-0.8R, 0.7-0.9R. Looking at the figures it can be observed that at low airspeeds the AGF system moves the theta quickness envelopes to the right. At high airspeeds the envelopes are moved to the left, but only marginally so. The effects increase as the AGF is moved outwards and the dynamic pressure increases. The same effect is evident also in Figure 33. which plots the peak pitch rate as a function of peak pitch attitude for the AGF position 0.6-0.8R. At low airspeed the AGF increases the maximum pitch rate, while at high airspeed it decreases the maximum pitch rate, slightly degrading the handling qualities.

Secondly, consider the effect of the AGF spanwise location on the theta quickness parameter. Figure 34 and Figure 35 present

the effect of spanwise location on the quickness charts for hover and 132 kts forward flight. A spanwise location of 0.3-0.5R is indicated in the legend as '35'. It can be seen that for lower airspeeds it is beneficial to position the AGF outboard on the blade, as this moves the quickness to the right towards improved HQs.

Next, consider the effect of the AGF deployment schedule on theta quickness. Figure 36 presents the general trend when varying the deployment as indicated in Table 4 for different airspeeds, assuming that the AGF system is located between 0.6-0.8*R*. As the airspeed is increased the quickness moves to the left from Level 1 to Level 2 HQs, increasing quickness. Figure 37 and Figure 38 narrow down the effect of actuation scheme on attitude quickness for the cases of hover and 132 kts forward flight. Observe that a deployment on the advancing side results in a decrease in quickness and performance. However, a deployment on the retreating side combined with an improper actuation phase may have the same effect. A deployment on the retreating side combined with an appropriate actuation phase results in an increased theta quickness and an improvement in handling qualities.

Table 4: Parametric variation of the AGF deployment schedule (r_{AGF} = 0.6-0.8R)

Deployment azimuth ψ_{out}	60°,120°,180°, 240°, 300°, 360°
Deployed period $\Delta\psi = \psi_{in} - \psi_{out}$	30°,60°,90°, 120°,150°,180°

Finally, the load quickness factor was also applied to the AGF rotor as seen in Figure 39. One can see that the introduction of the AGF system results in an increase in the vibratory loads. For the pulse manoeuvre, this corresponds to an increase in the 4/rev hub shear vibratory component.

4 CONCLUSIONS

Concerning the unsteady aerodynamics of the AGF system it can be concluded that:

1. The two empirical models employed by CIRA and NLR display an acceptable correlation with respect to 2-D URANS CFD computations, even when considering an unsteady free-stream. Future wind tunnel test activities will allow for a further validation of the models.

2. The model adopted by NLR requires a relatively large amount of CFD or measurement data to define the steady state response, which shows significant airfoil dependency. The tuning of the unsteady terms appears far less sensitive to airfoil type.

Related to the performance of the AGF system it can be stated that:

1. Maximum power reductions on the investigated configuration are achieved when positioning the AGF system at 70-90% of the blade radius.

2. When deployed over the retreating side of the rotor disk, the AGF system works to off-load the retreating blade tip and reduce the angle of attack over a large part of rotor disk. The combined effect compensates for the additional torque generated over the span of the AGF system and produces a net power reduction.

3. Straightforward open-loop control scheduling can be applied to achieve significant power reductions across the level flight envelope without increasing the 4/rev vibrations.

Concerning the handling qualities of a helicopter equipped with a generic AGF rotor it can be concluded that:

5 An AGF system introduced to improve performance moves the quickness in pitch towards Level 1 HQs at low airspeeds. At high airspeeds the AGF moves the theta quickness towards Level 2 HQs, but the effect is less pronounced.

6 Outboard placement of the AGF system increases its effectiveness and therefore also its effect on handling qualities.

7 Deployment on the advancing side results in a decrease in theta quickness and performance. However, a deployment on the retreating side combined with an improperly selected actuation phase may have the same effect. Deployment on the retreating side combined with an appropriate actuation phase results in increased quickness.

5 FUTURE RESEARCH

In the course of 2013 the first experimental data will become available. The continuation of the project will see both static and oscillating airfoil experiments, as well as a model rotor test and eventually a flight test campaign. All of these test activities will provide valuable data that can be used to validate the numerical models in representative environments. In parallel, future analysis activities will investigate closed-loop control solutions such as adaptive Higher Harmonic Control, also considering higher deployment frequencies, to compare these to the open-loop strategies developed thus far.

6 ACKNOWLEDGEMENTS

7 REFERENCES

Liebeck, R.H., "Design of Subsonic Airfoils for High Lift", Journal of Aircraft, Vol. 15(9), pp. 547-561, 1978.

1. Kinzel, M.P., "Miniature Trailing-Edge Effectors for Rotorcraft Performance Enhancement", Proceedings of the American Helicopter Society 61st Annual

Forum, Grapevine, Texas, May 2005, pp. 442-453.

2. Roedts, R.L and Maughmer, M.D., "Rotorcraft Performance Enhancements Due to a Lower-Surface Effector", Proceedings of the 35th European Rotorcraft Forum, Hamburg, Germany, September 2009, pp. 886-899.

3. Bae, E.S., Gandhi, F. and Maughmer, M., "Optimumly Scheduled Deployments of Miniature Trailing-Edge Effectors for Rotorcraft Power Reduction", Proceedings of the American Helicopter Society 65th Annual Forum, Grapevine, Texas, May 2009, pp. 187-211.

4. Padthe, A. K., Liu, L. and Friedmann, P., "Numerical Evaluation of Microflaps for On Blade Control of Noise and Vibration", AIAA Paper 2011-1873.

5. Bae, E.S. and Gandhi, F., "Upstream Active Gurney Flap for Rotorcraft Vibration Reduction", Proceedings of the American Helicopter Society 68th Annual Forum, Fort Worth, Texas, May 2012, pp. 1354-1362.

6. Liu, L., Friedmann, P.P., Kim, I. and Bernstein, D.S., "Rotor Performance Enhancement and Vibration Reduction in Presence of Dynamic Stall Using Actively Controlled Flaps", Proceedings of the American Helicopter Society 62nd Annual Forum, Phoenix, Arizona, June 2006, pp. 986-998.

7. Vieira, B.A.O., Kinzel, M.P. and Maughmer M.D., "Unsteady Aerodynamics of Miniature Trailing-Edge Effectors Based on Indicial Methods", AIAA Paper 2011-1049.

8. Hariharan, N. and Leishman, J.G., "Unsteady Aerodynamics of a Flapped Airfoil in Subsonic Flow by Indicial Concepts", AIAA Paper 1995-1228.

9. Leishman, J.G., and Beddoes, T.S., "A Generalized Model for Airfoil Unsteady Aerodynamic Behavior and Dynamic Stall Using the Indicial Method," presented at the 42nd American Helicopter Society Annual Forum, 2-5 June1986;

10. He, C., Du Val, R.W., "A Unsteady Airload Model with Dynamic Stall for Rotorcraft Simulation," Proceedings of the 50th American Helicopter Society Annual Forum, Washington, D.C., May 1994.

11. He, C., "A Study of Rotor Loads and Response with Dynamically Cambered Blades," Proceedings of the American Helicopter Society 2nd International Aeromechanics Specialists' Conference, Bridgeport, Connecticut, October 1995.

12. Catalano, P., and Amato, M., "An Evaluation of RANS Turbulence Modelling for Aerodynamic Applications," Aerospace Science and

Technology Journal, Vol.7, pp. 493-509, 2003.

13. Marongiu, C., "On the Aerodynamic Force of Oscillating Airfoils," Ph.D. Dissertation, University of Naples, Federico II, 2009.

14. A. le Pape, Richter, K., Knopp, T., Costes, M., Gleize, V. and Gardner, A.D., "Validation of Structured and Hybrid Numerical Methods for Improved two-Dimensional Dynamic Stall Prediction", presented at the 10th ONERA-DLR Aerospace Symposium, Berlin, Germany, 2009.

15. Kok, J.C., Boerstoel, J.W., Kassies A., and Spekreijse S.P., "A Robust Multi-Block Navier-Stokes Flow Solver for Industrial Applications", Proceedings of ECCOMAS Conference, Paris, France, 1996.

16. Kok, J.C., "Resolving the dependence on freestream values for the k-ω turbulence model", AIAA Journal, 38(7), pp. 1292–1294, 2000.

17. Dol, H.S., Kok, J.C., and Oskam, B., "Turbulence Modelling for Leading-Edge Vortex Flows", AIAA Paper 2002-0843.

18. Van der Wall, B.G. and Leishman, J.G., "The Influence of Variable Flow Velocity on Unsteady Airfoil Behavior", Proceedings of the 18th European Rotorcraft Forum, Avignon, France, September 1992.

19. Johnson, W., "Rotorcraft Aerodynamics Models for a Comprehensive Analysis", Presented at the 54th American Helicopter Society Annual Forum, Washington, DC, May 1998.

20. Lee, H. and Kroo, I.M., "Computational Investigation of Wings with Miniature Trailing Edge Control Surfaces", AIAA Paper 2004-2693.

21. Pavel, M. D., "On the Necessary Degrees of Freedom for Helicopter and Wind Turbine Low-Frequency Mode Modelling", Ph.D. Dissertation, Delft University of Technology, 2001.

22. Van Holten, T., "On the Validity of Lifting Line Concepts in Rotor Analysis", Vertica, vol.1, pp. 239-254, 1977.

23. Van Holten, T., "Upgrading of Classical Lifting-Line Theory to Obtain Accurate Flight Mechanical Helicopter models: Improved Correction for Sweep Effects" AGARD-FVP Symposium Advances in Rotorcraft Technology, Ottawa, Canada, May 1996.

24. Forrester, A.I.J, Sóbester, A. and Keane, A.J., "Engineering Design via Surrogate Modelling: A Practical Guide", American Institute of Aeronautics and Astronautics, 2008.

25. Svenson, J.D., "Computer Experiments: Multiobjective Optimisation and Sensitivity Analysis", The Ohio State University, 2011.

26. "Handling Qualities Requirements for Military Rotorcraft, Performance Specification, ADS-33-PRF", USAAMC, Aviation Engineering Directorate, March 2000.

27. Padfield, G.D., "Helicopter Flight Dynamics", Blackwell Science LTD., Second Edition. 2007.

28. Pavel. M.D., Padfield, G., "ADS-33 metrics for Agility Enhancement and Structural Loads Alleviation", Journal of the American Helicopter Society, Vol. 51, No.4, Oct 2006, pp. 319-330.
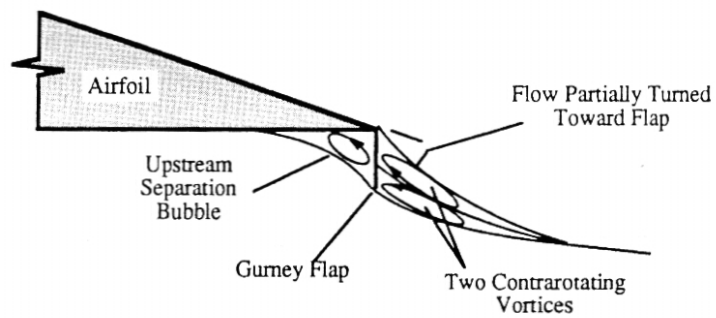
Figure 1: Gurney flap concept[1]
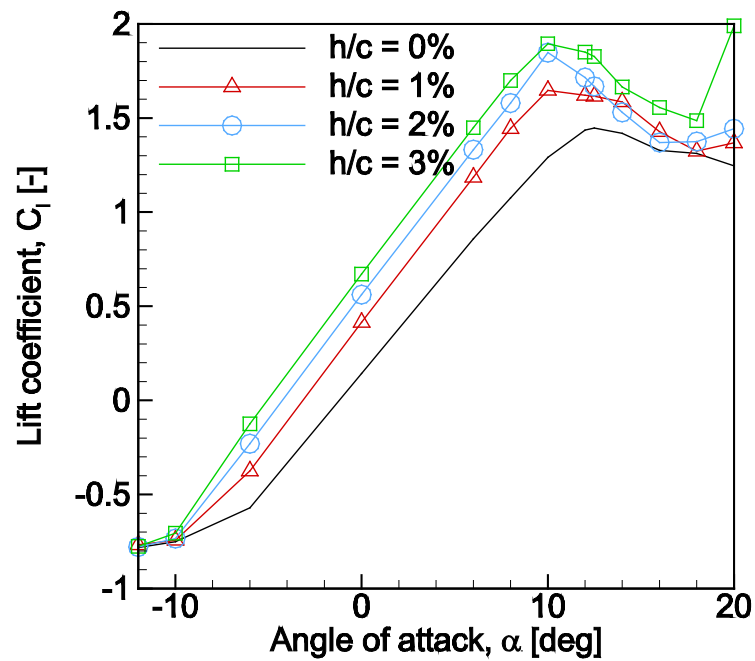
Figure 2: Lift coefficient for NACA-23012 airfoil with upstream Gurney flap, M = 0.4
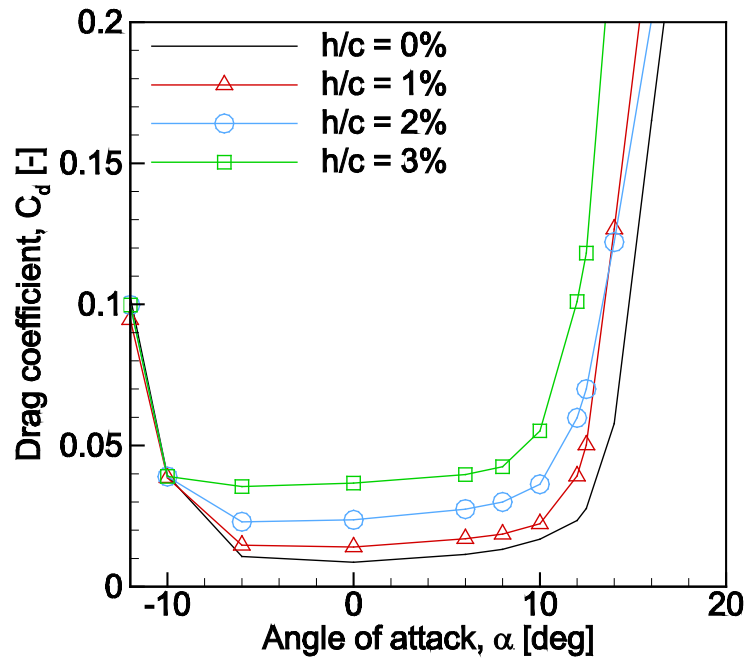
Figure 3: Drag coefficient for NACA-23012 airfoil with upstream Gurney flap, M = 0.4
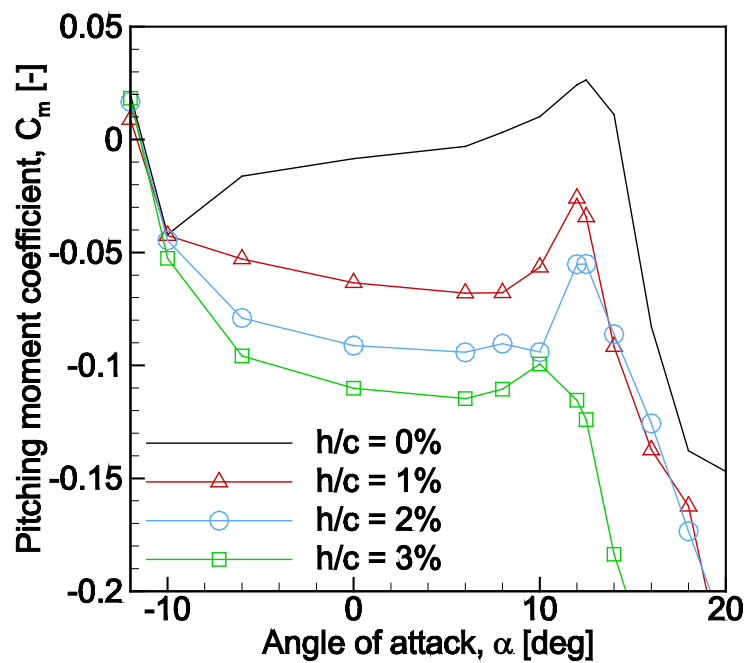
Figure 4: Pitching moment coefficient for NACA-23012 airfoil with upstream Gurney flap, M = 0.4
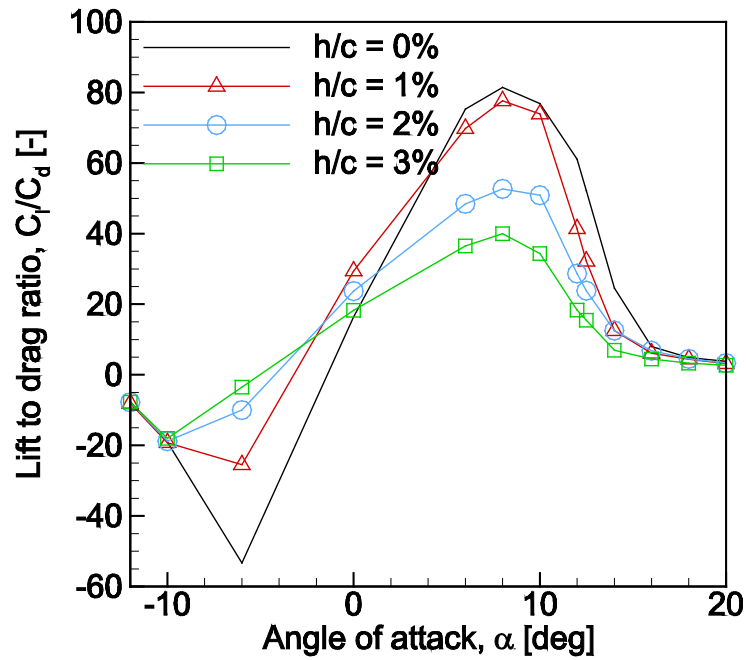
Figure 5: Lift to drag ratio for NACA-23012 airfoil with upstream Gurney flap, M = 0.4
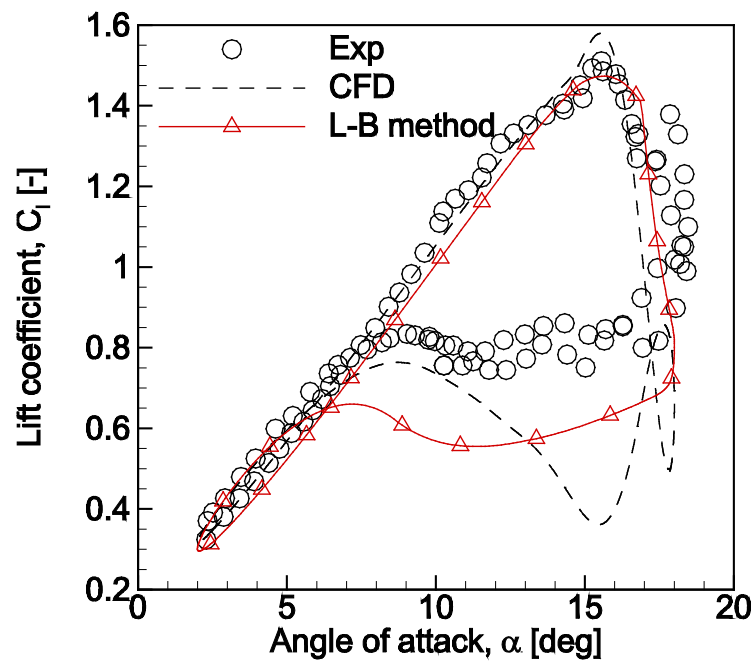
Figure 6: Dynamic stall cycle on clean NACA-0012 airfoil: lift coefficient, M = 0.4
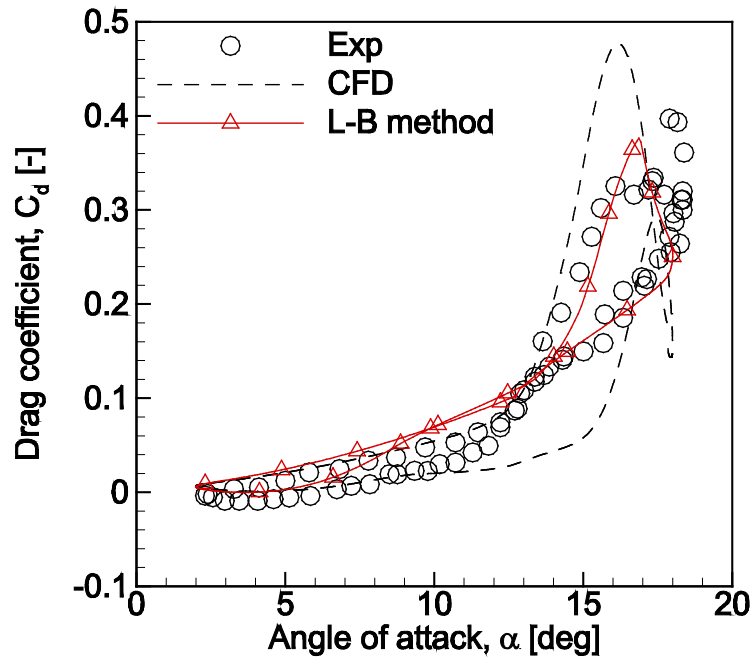
Figure 7: Dynamic stall cycle on clean NACA-0012 airfoil: drag coefficient, M = 0.4
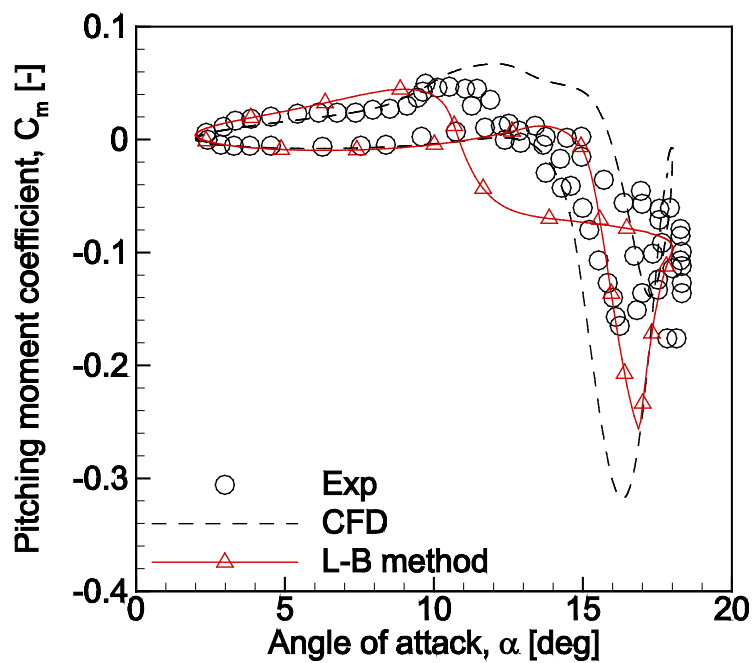
Figure 8: Dynamic stall cycle on clean NACA-0012 airfoil: pitching moment coefficient,
M = 0.4
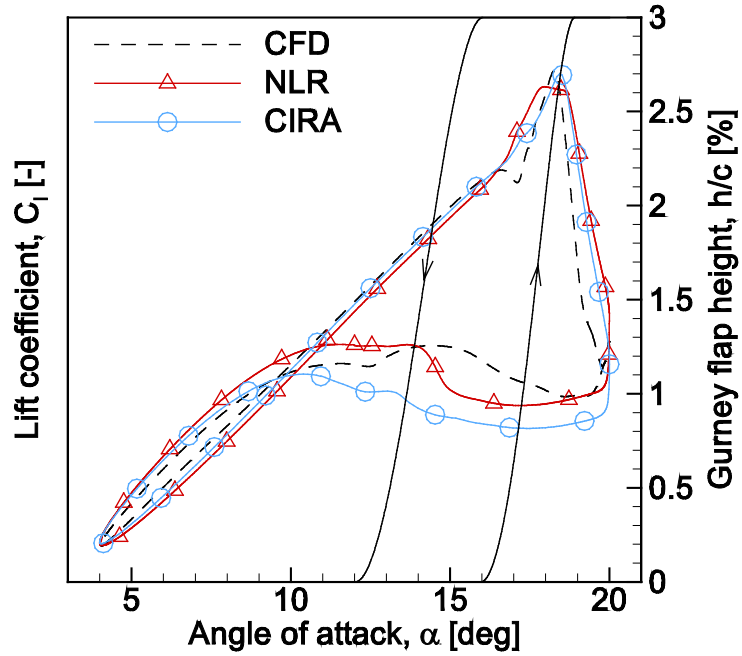
Figure 9: Dynamic stall cycle on ARO-212 airfoil with AGF deployment: lift coefficient, M = 0.4
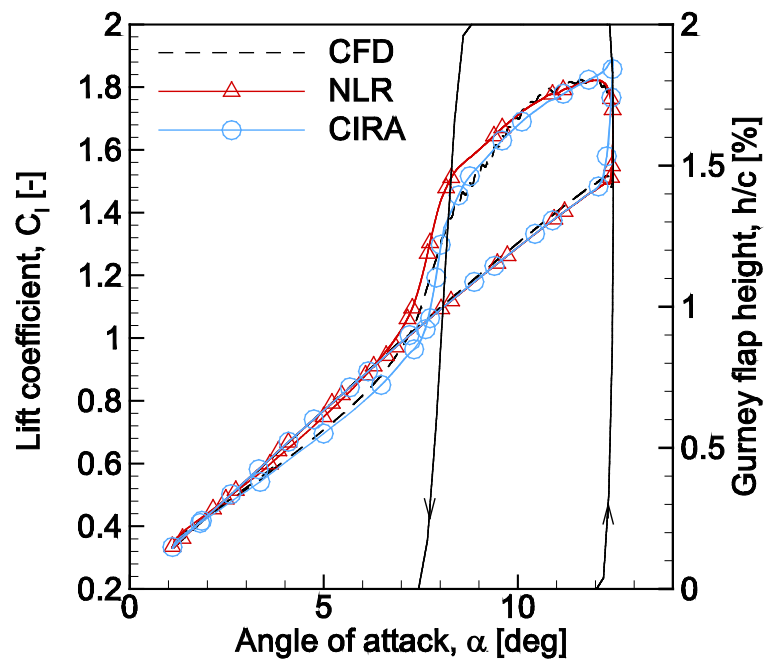
Figure 10: Lift on an oscillating NACA-23012 airfoil in a time-varying freestream
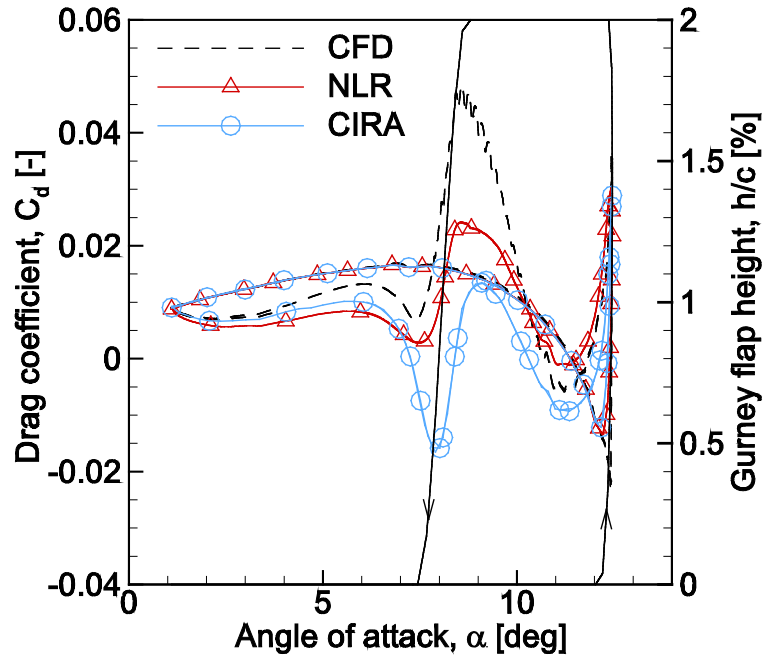
Figure 11: Drag on an oscillating NACA-23012 airfoil in a time-varying freestream
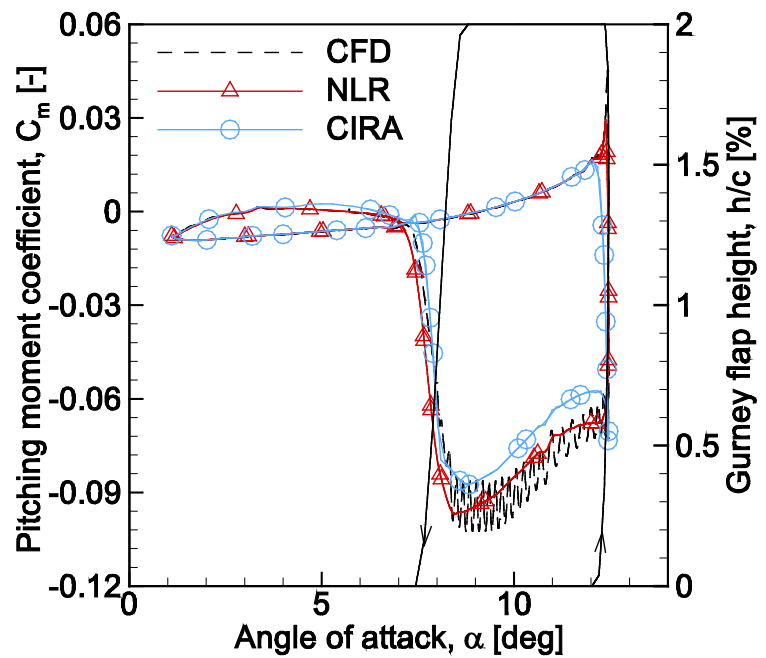
Figure 12: Pitching moment on an oscillating NACA-23012 airfoil in a time-varying freestream
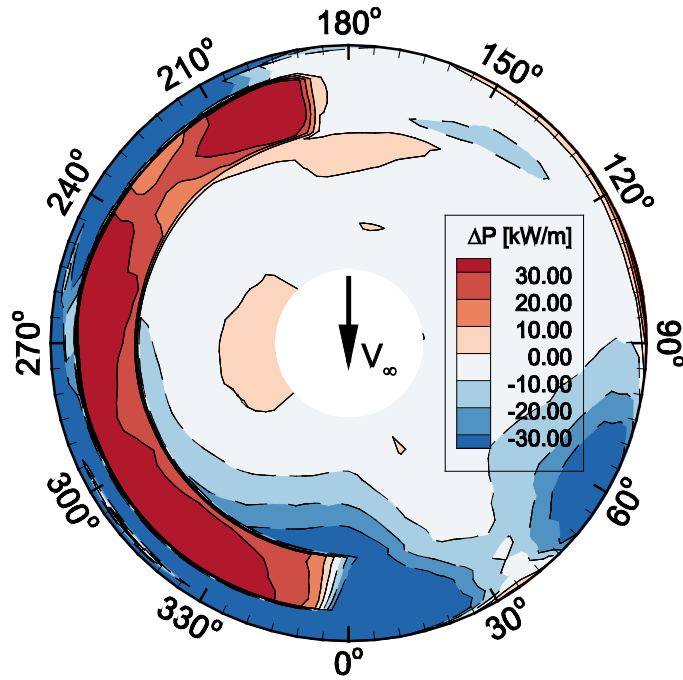
Figure 13: Power difference in condition J_1: $\Delta P = P_{active} - P_{baseline}$
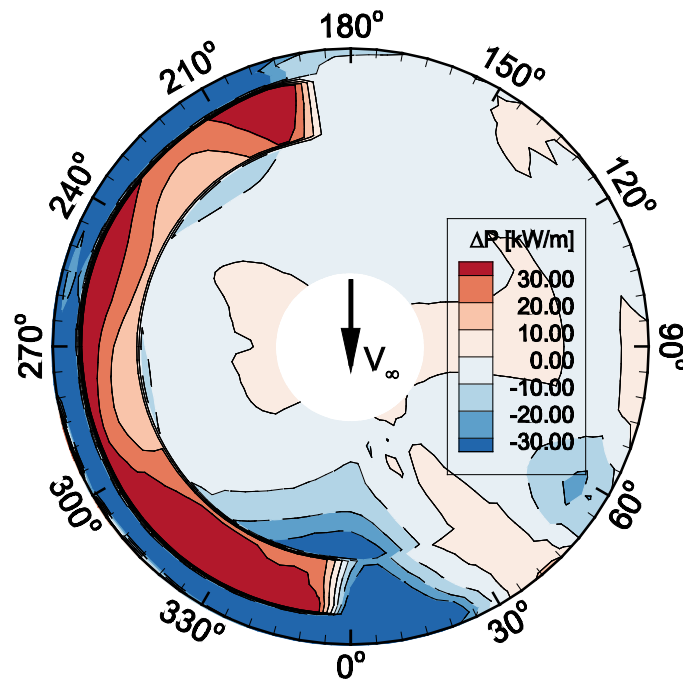
Figure 14: Power difference in condition J_2: $\Delta P = P_{active} - P_{baseline}$
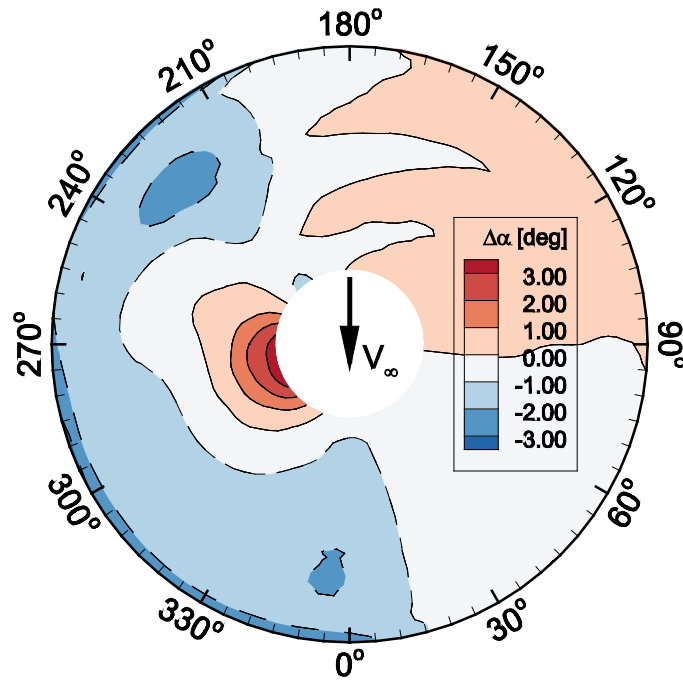
Figure 15: Angle of attack difference in condition J_1: $\Delta\alpha = \alpha_{active} - \alpha_{baseline}$
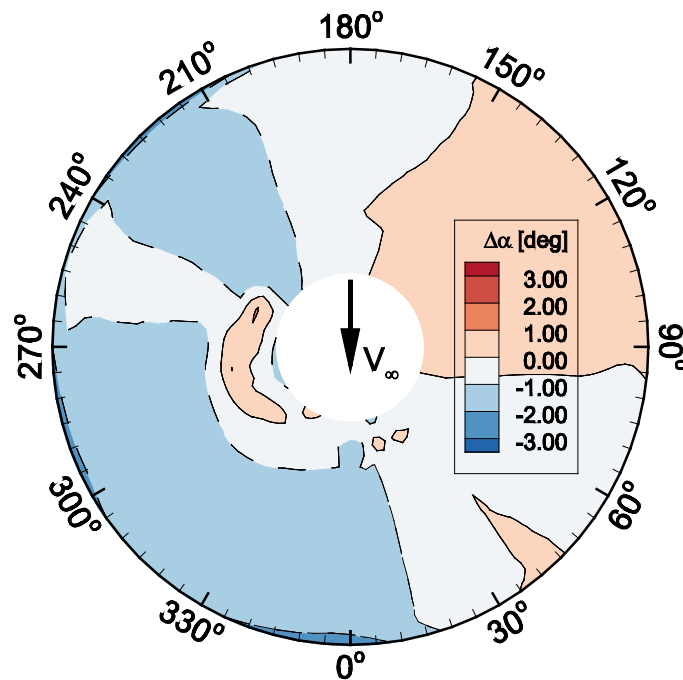
Figure 16: Angle of attack difference in condition J_2: $\Delta\alpha = \alpha_{active} - \alpha_{baseline}$
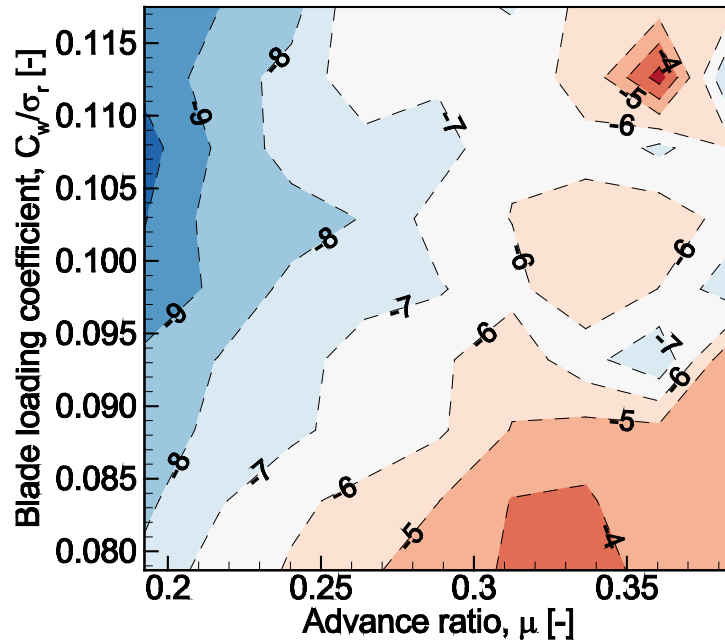
Figure 17: Unscheduled power difference: $\Delta P = P_{active} - P_{baseline}$ [%]
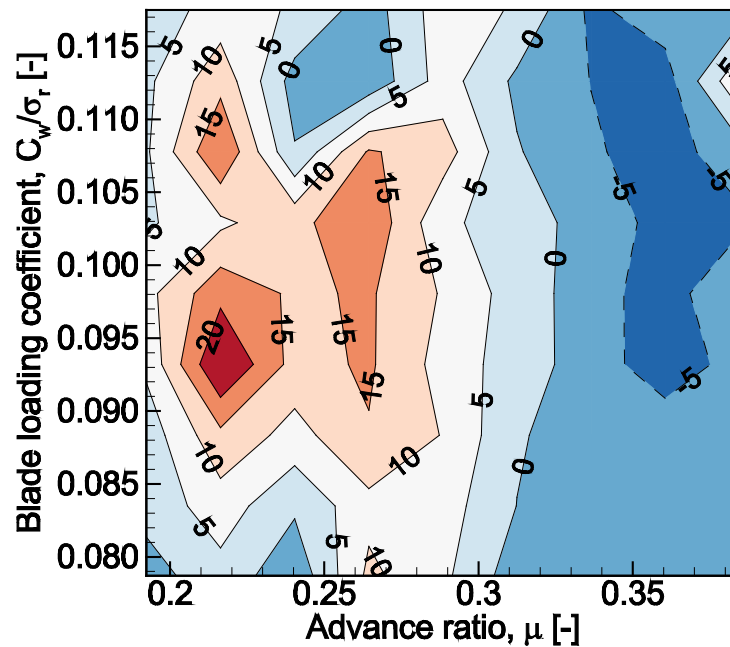
Figure 18: Unscheduled difference in 4/rev pilot seat vibrations: $\Delta \ddot{x}^{4P} = \ddot{x}^{4P}_{active} - \ddot{x}^{4P}_{baseline}$ [%]
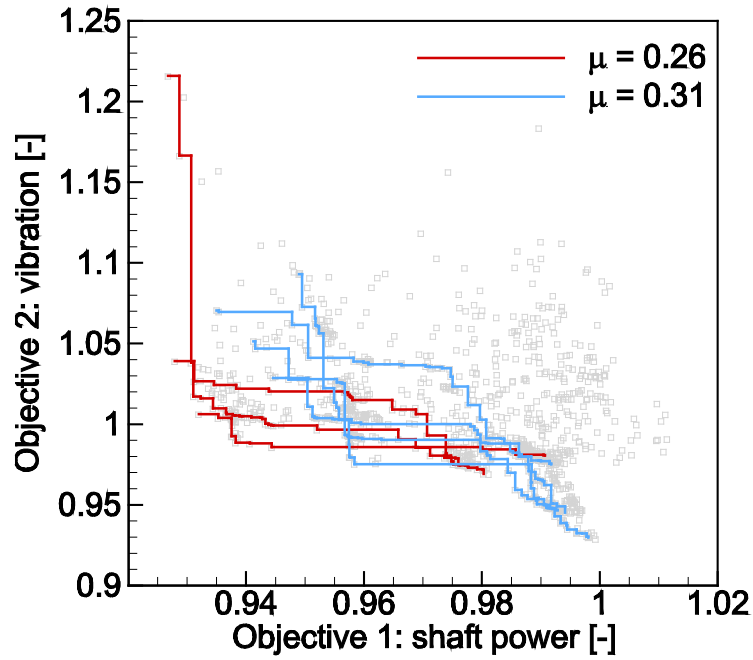
Figure 19: Sample of Pareto fronts of local optimisations
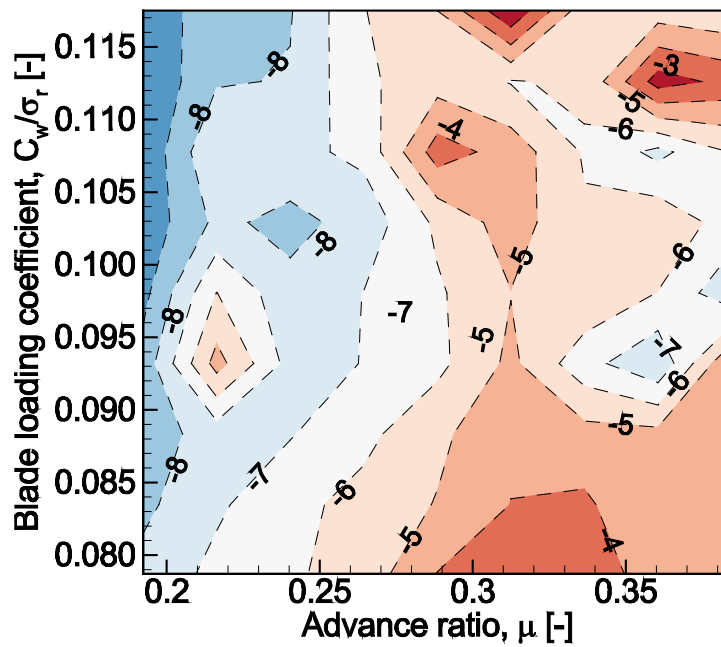
Figure 20: Scheduled power difference: $\Delta P = P_{active} - P_{baseline}$ [%]
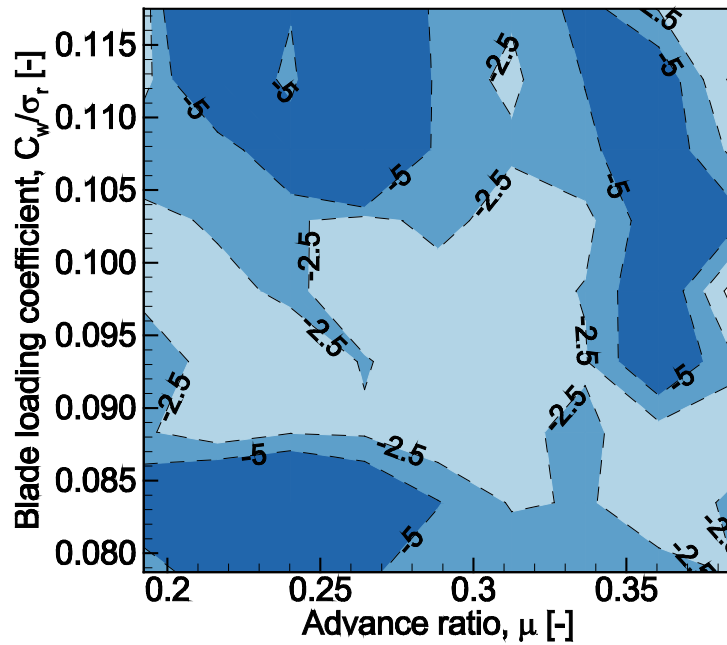
Figure 21: Scheduled difference in 4/rev pilot seat vibrations: $\Delta\ddot{x}^{4P} = \ddot{x}^{4P}_{active} - \ddot{x}^{4P}_{baseline}$ [%]
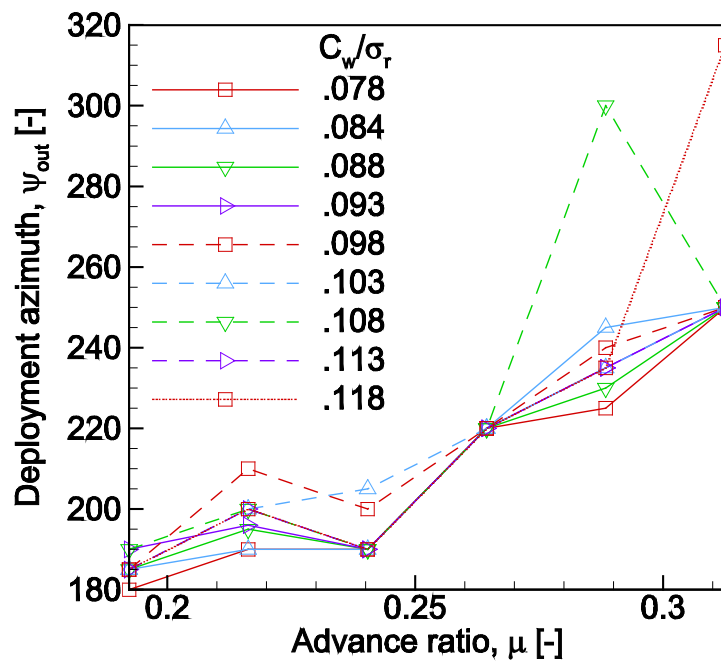
Figure 22: Open-loop AGF deployment schedule, deployment azimuth ψ_{out}

35
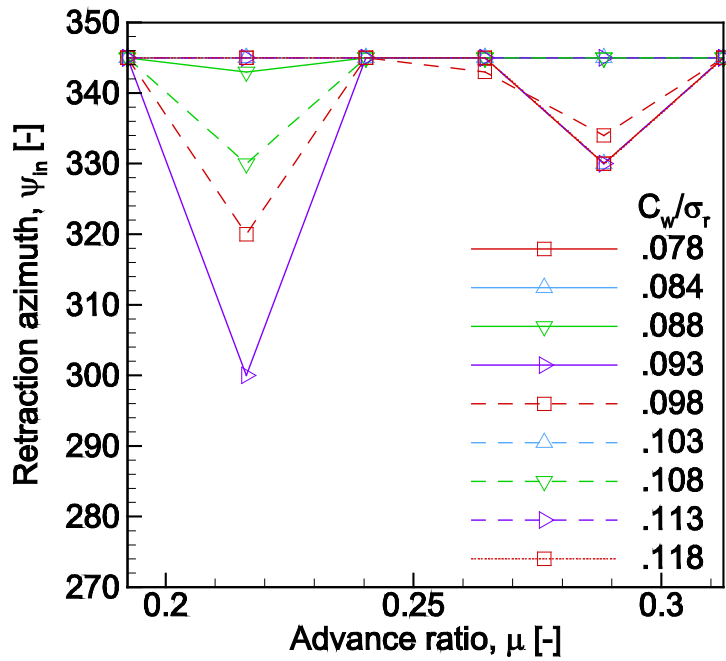
Figure 23: Open-loop AGF deployment schedule, retraction azimuth ψ_{in}
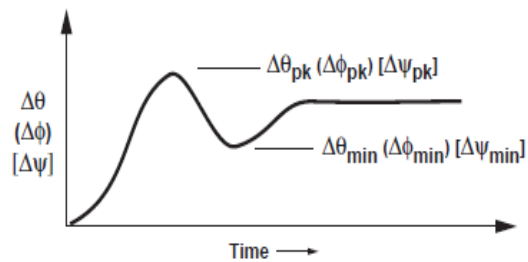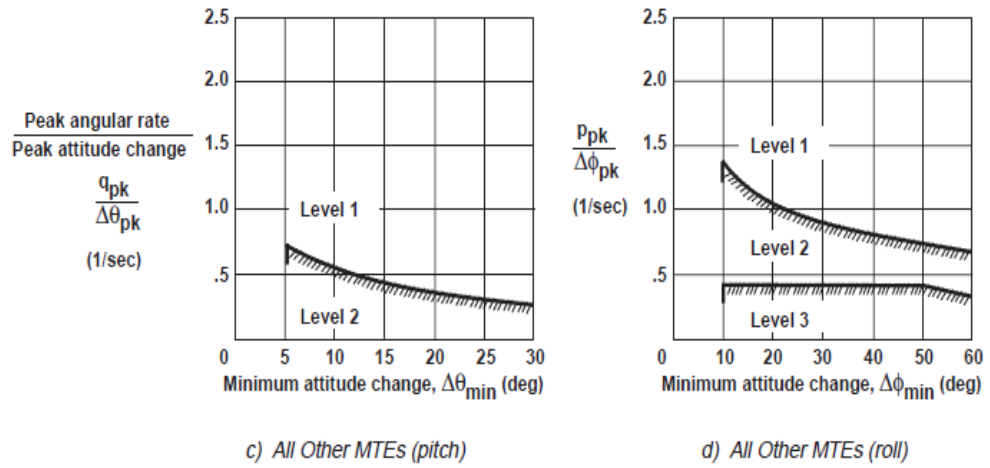
Figure 24: Definition of ADS-33 attitude quickness parameter

36
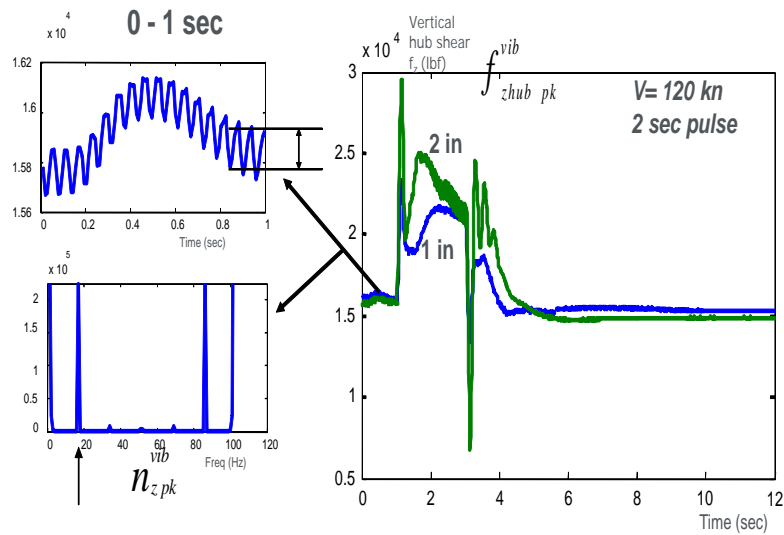
Figure 25: Definition of vibratory load quickness parameter
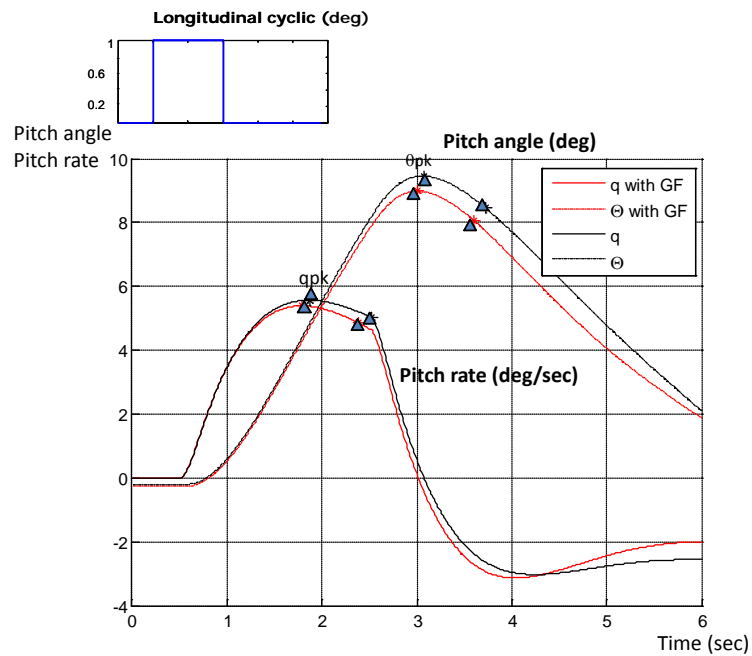
Figure 26: Helicopter response to longitudinal cyclic input, V = 132 kts, 2 sec duration 1° pulse
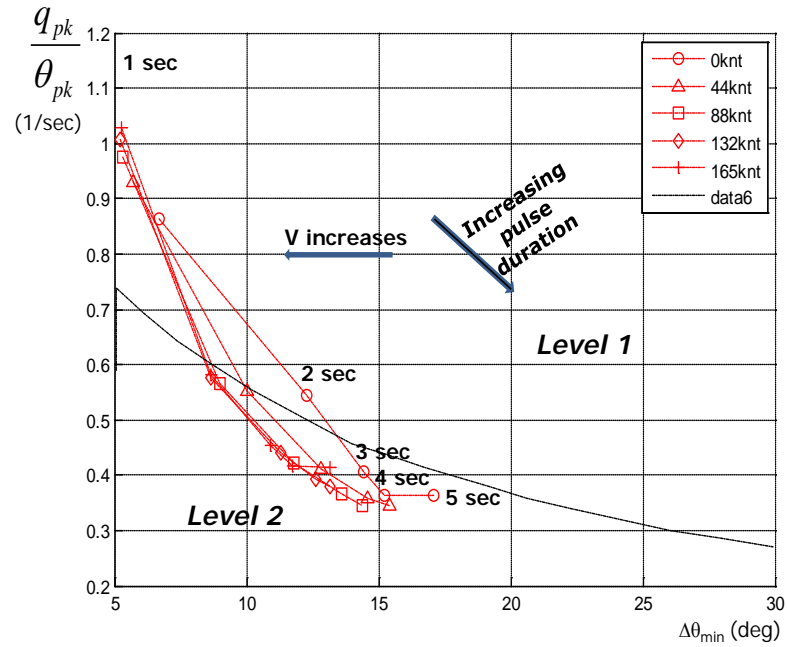
Figure 27: Attitude quickness parameter for pull-up manoeuvres, baseline rotor, pulses of 1°
longitudinal cyclic varying from 1-5 sec
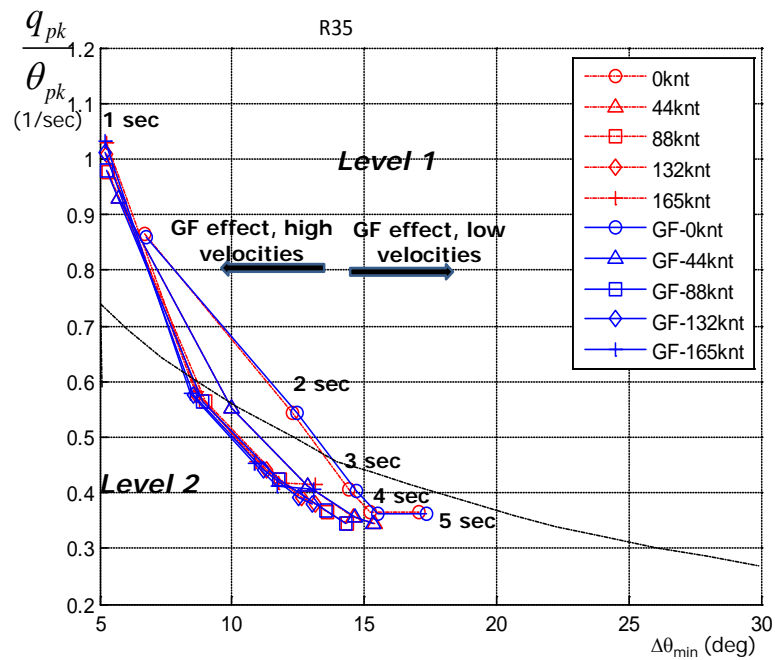
Figure 28: AGF effect on quickness, r_{AGF} = 0.3-0.5R, ψ_{out} = 210-220°, ψ_{in} = 330-340°
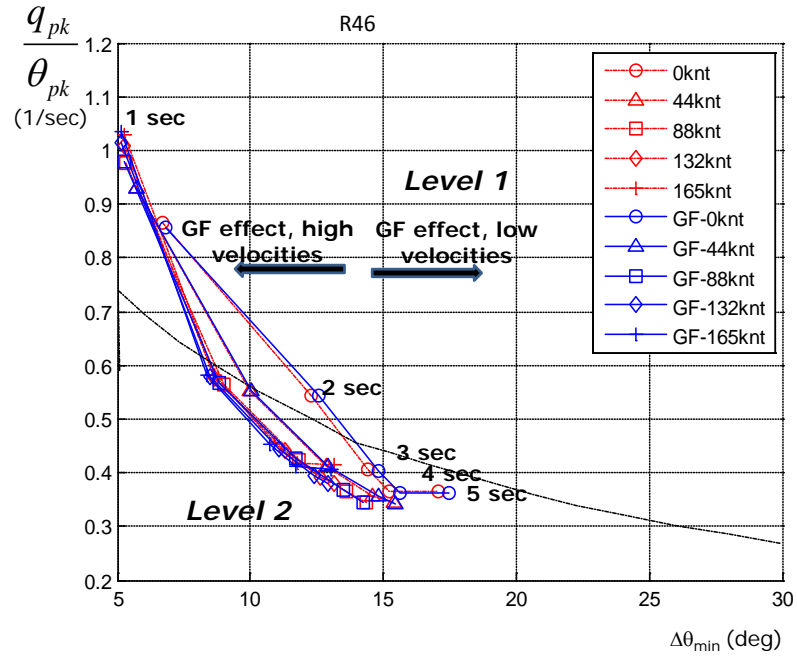
Figure 29: AGF effect on quickness, $r_{AGF} = 0.4\text{-}0.6R$, $\psi_{out} = 210\text{-}220°$, $\psi_{in} = 330\text{-}340°$
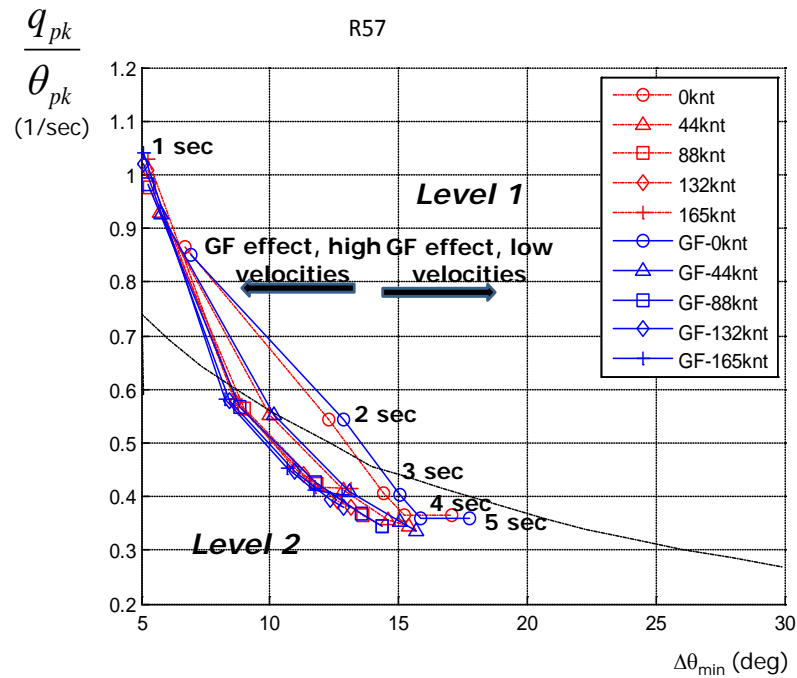
Figure 30: AGF effect on quickness, $r_{AGF} = 0.5\text{-}0.7R$, $\psi_{out} = 210\text{-}220°$, $\psi_{in} = 330\text{-}340°$
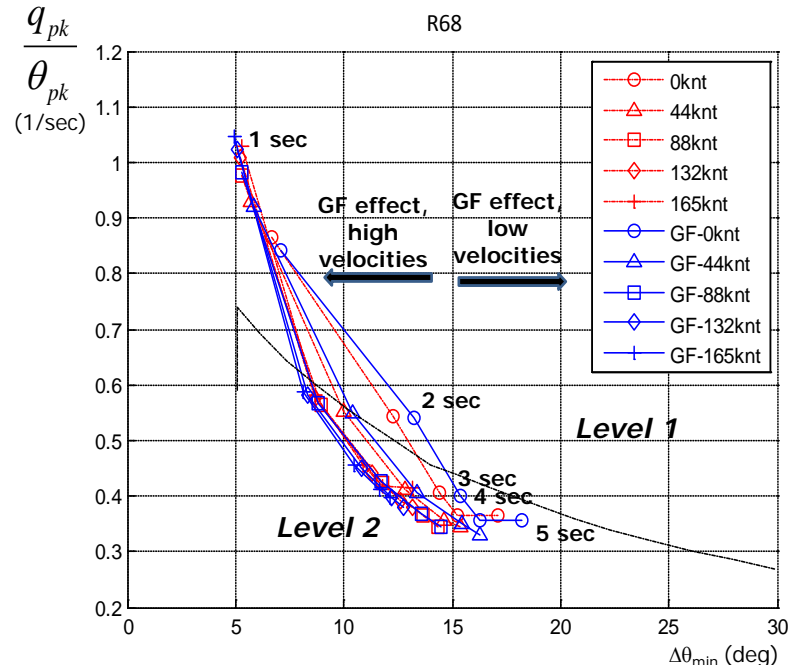
Figure 31: AGF effect on quickness, $r_{AGF} = 0.6\text{-}0.8R$, $\psi_{out} = 210\text{-}220°$, $\psi_{in} = 330\text{-}340°$
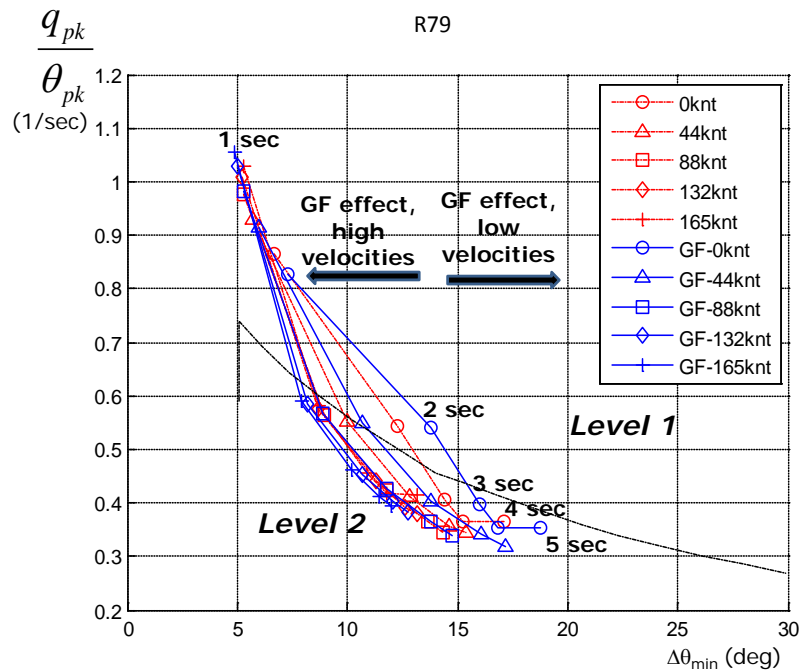
Figure 32: AGF effect on quickness, $r_{AGF} = 0.7\text{-}0.9R$, $\psi_{out} = 210\text{-}220°$, $\psi_{in} = 330\text{-}340°$
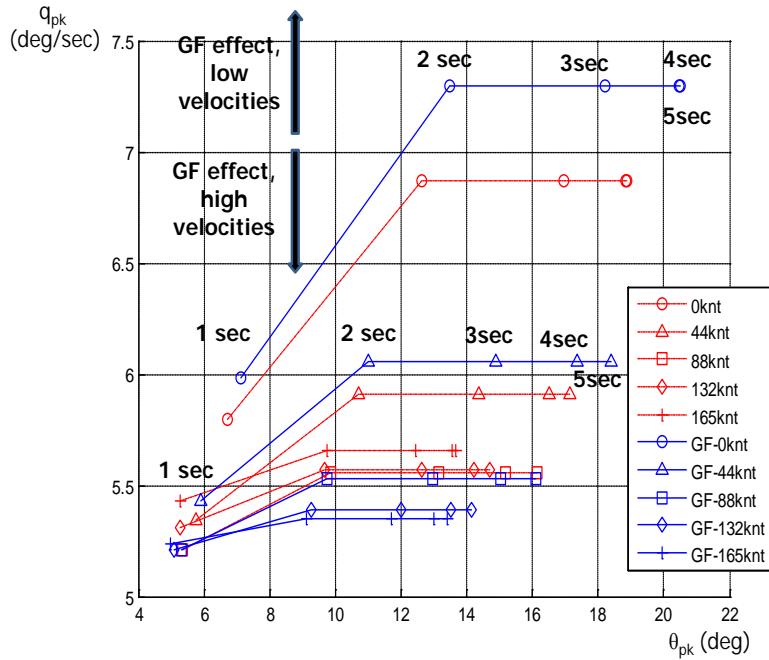
Figure 33: AGF effect on maximum pitch rate, $r_{AGF} = 0.6\text{-}0.8R$, $\psi_{out} = 210\text{-}220°$, $\psi_{in} = 330\text{-}340°$
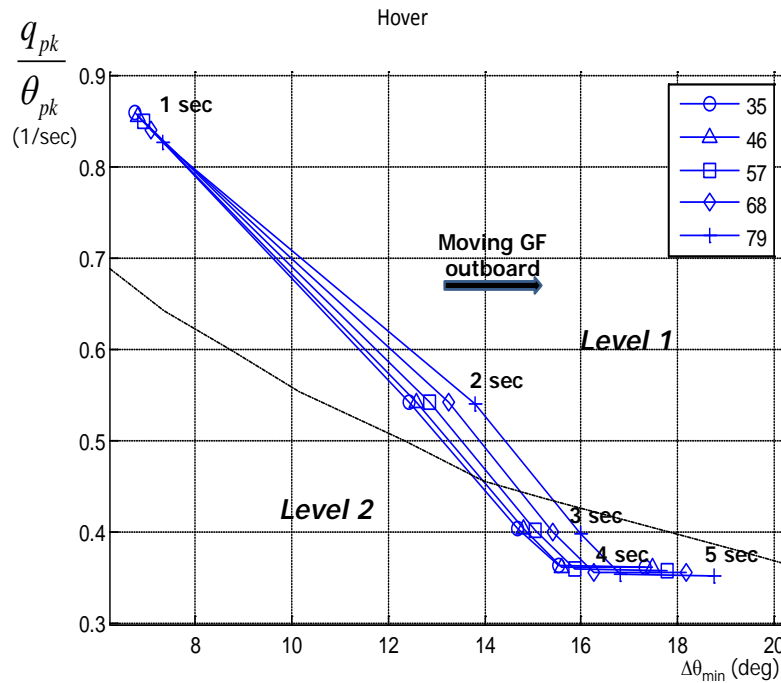
Figure 34: Effect of AGF spanwise location on quickness, hover, $\psi_{out} = 210\text{-}220°$,
$\psi_{in} = 330\text{-}340°$
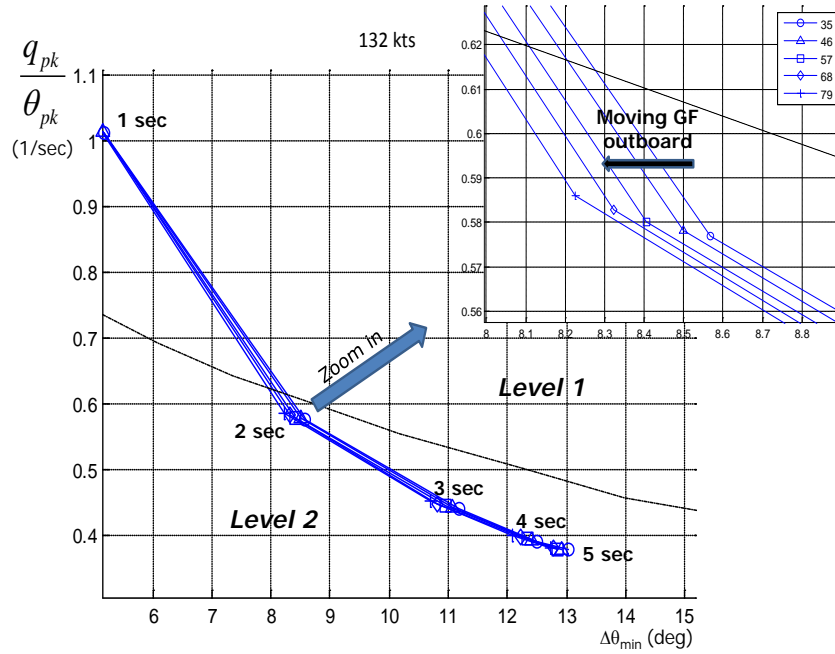
Figure 35: Effect of AGF spanwise location on quickness, V = 132 kts, ψ_{out} = 210-220°, ψ_{in} = 330-340°
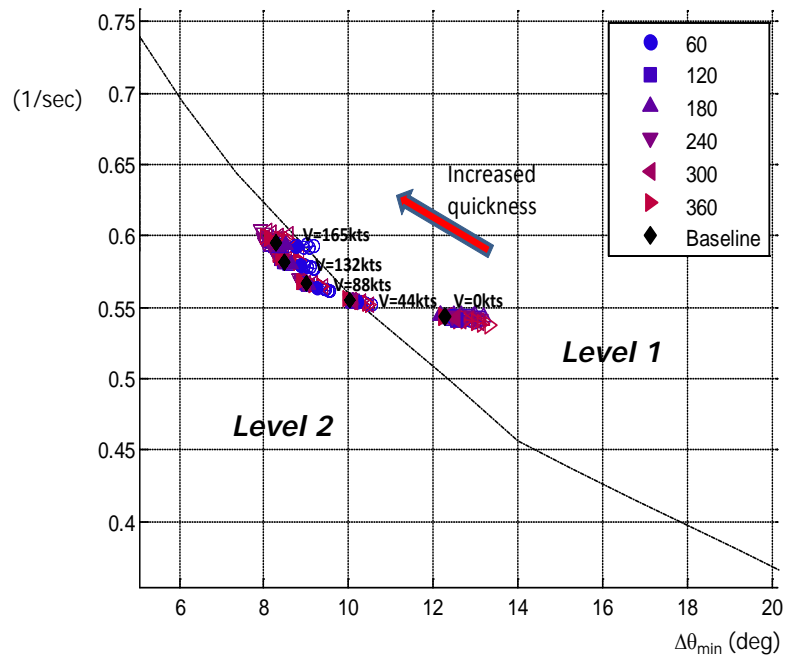
Figure 36: Effect of AGF actuation schedule on quickness, r_{AGF} = 0.6-0.8R
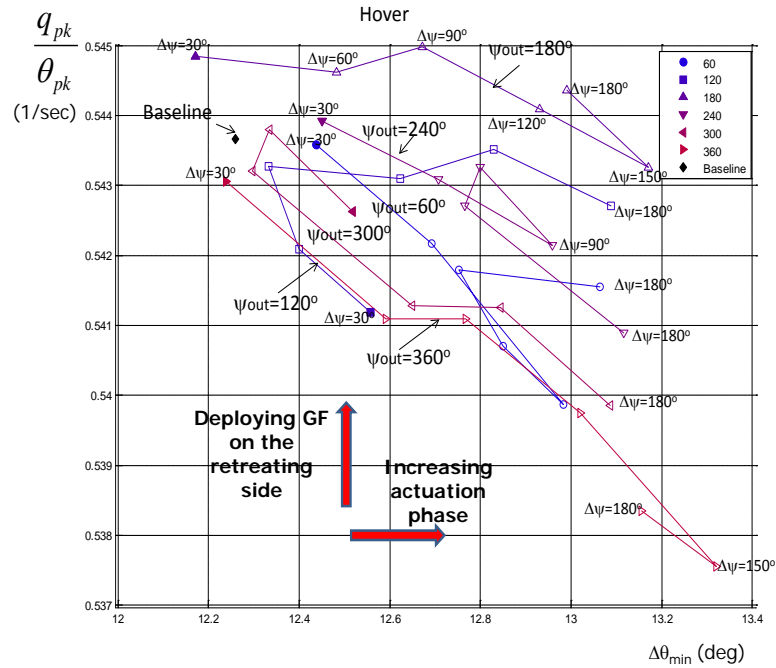
Figure 37: Effect of AGF schedule on quickness, hover, r_{AGF} = 0.6-0.8R, variation in ψ_{out} and $\Delta\psi$
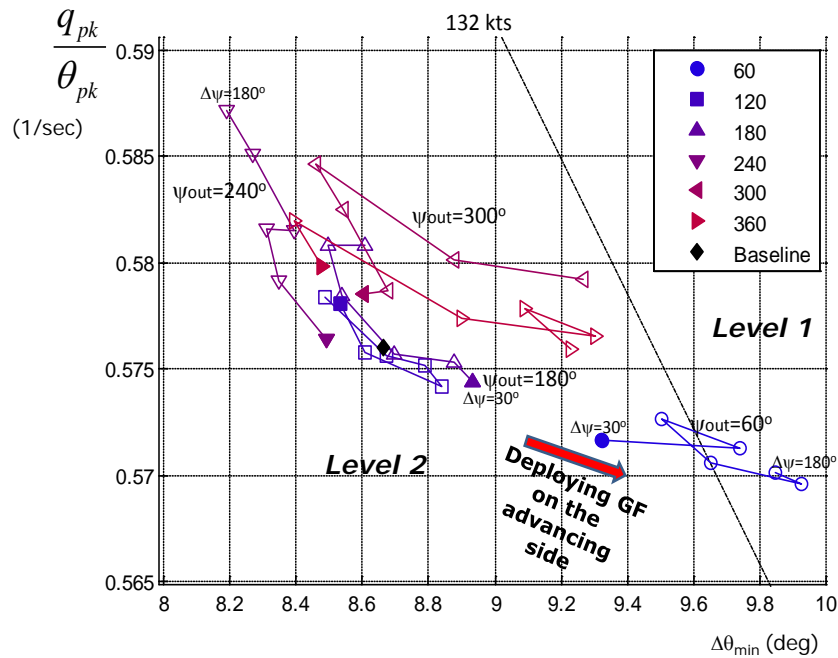

Figure 38: Effect of AGF schedule on quickness, V = 132 kts, r_{AGF} = 0.6-0.8R, variation in ψ_{out} and $\Delta\psi$
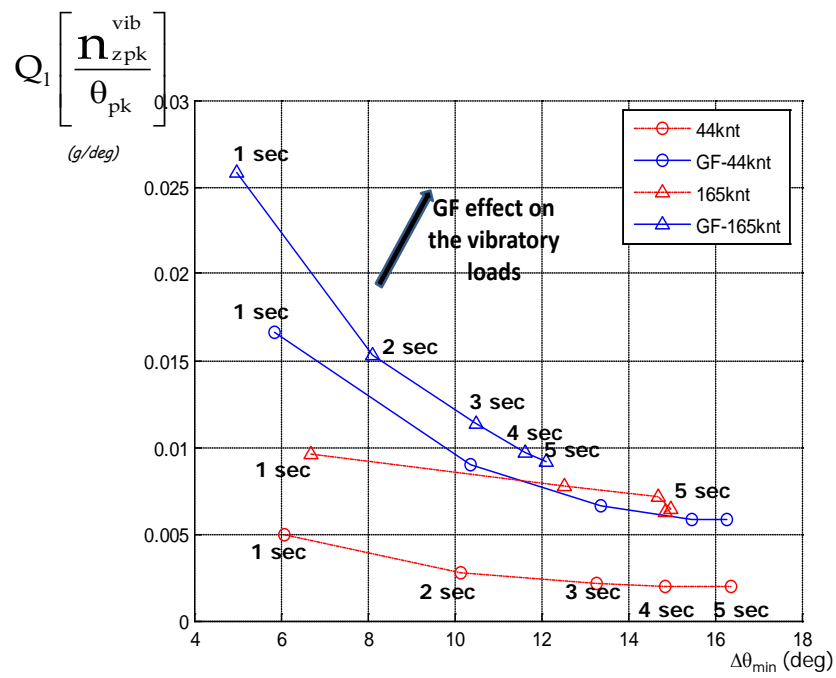
Figure 39: Vibratory quickness chart for V = 44-165 kts, r_{AGF} = 0.6-0.8R, ψ_{out} = 210-220°, ψ_{in} = 330-340°